Non-standard interactions and the CP phase measurements in neutrino oscillations at low energies

Shao-Feng Ge* and Alexei Yu. Smirnov†

Max-Planck-Institut für Kernphysik, Saupfercheckweg 1, Heidelberg 69117, Germany

September 29, 2016

Abstract

We study the effects of non-standard interactions (NSI) and the genuine CP phase δ_D in neutrino oscillations at low, $E_\nu \lesssim 1\,\text{GeV}$, and very low, $E_\nu \lesssim 0.1\,\text{GeV}$, energies. For experimental setup with baseline and neutrino energy tuned to the first 1-3 oscillation maximum, we develop a simple analytic formalism to show the effects of NSI. The vacuum mimicking and its violation as well as the use of the separation basis play a central role in our formalism. The NSI corrections that affect the CP phase measurement mainly come from the violation of vacuum mimicking as well as from the corrections to the 1-3 mixing angle and mass-squared difference. We find that the total NSI correction to the $\nu_\mu - \nu_e$ probability $P_{\mu e}$ can reach $20\% - 30\%$ (1σ) at T2(H)K. Correspondingly, the correction to the CP phase can be as large as $50°$ and hence significantly deteriorates the CP sensitivity at T2(H)K. The proposed TNT2K experiment, a combination of T2(H)K and the short baseline experiment μKam that uses the Super-K/Hyper-K detector at Kamioka to measure the oscillation of the antineutrinos from muon decay at rest (μDAR), can substantially reduce the degeneracy between NSI and the genuine CP phase δ_D to provide high CP sensitivity. The NSI correction to $P_{\mu e}$ is only 2% (1σ) for μDAR neutrinos.

1. Introduction

The determination of the Dirac CP phase, δ_D, and searches for new (non-standard) neutrino interactions [1], [2, 3] are among the main objectives of present-day neutrino physics (see [4, 5] for reviews). There are certain connections between the two unknowns:

- NSI can be additional source of CP violation on top of the PMNS matrix [6, 7].

---

*gesf02@gmail.com

†smirnov@mpi-hd.mpg.de

- The effects of NSI and CP violation are entangled in oscillation experiments, thus creating the δ_D-NSI degeneracy problem [7, 8].

Within the standard 3ν paradigm (no NSI, no sterile neutrinos, *etc.*), the global fit of oscillation data gives more than 2σ indication of CP violation with the best-fit value $\delta_D \approx 3\pi/2$. This indication follows mainly from the results of T2K [9] and NOνA [10] in combination with the results of reactor and some other experiments. The confirmation of this hint and measurement of the CP phase are associated to future experiments with neutrinos of different origins. The current T2K experiment can be extended to T2K-II [11, 12] by upgrading the flux and eventually to T2HK with a much larger Hyper-K detector [13], or even T2KK/T2KO [14, 15, 16, 17, 18, 19, 20, 21] with longer baseline. The DUNE [22, 23, 24] experiment should provide precision measurement of δ_D. In addition to accelerator experiments, the CP phase δ_D can also have large observable effect in the oscillation of atmospheric neutrinos below $1\,\mathrm{GeV}$. This can be explored using the future possible upgrades of PINGU and ORCA detectors with $3 \sim 4$ times denser instrumentation [25]. At even lower energy, $E_\nu \lesssim 0.1$ GeV, one can also employ neutrinos from the muon decay at rest (μDAR) in proposed experiments like DAEδALUS [26] and CI-ADS [27], or in-flight in experiments like MOMENT [28, 29] to measure δ_D. Measuring the antineutrino oscillation $\bar{\nu}_\mu \to \bar{\nu}_e$ from the μDAR source with the detector of JUNO/RENO-50, which is originally designed to establish the neutrino mass hierarchy, can also determine the CP phase [30].

Interpretation of the present results on CP violation can be affected by the possible presence of non-standard interactions [31] or sterile neutrinos [32, 33, 34]. The effects of NSI substantially reduce the sensitivity to δ_D at the ongoing T2K and NOνA experiments [35, 31, 36], and the future long-baseline experiments, in particular, DUNE [37, 38, 39, 35, 31, 40, 36, 41, 42, 43]. So, the problem is to disentangle the genuine CP violation and the NSI effects in a way that can guarantee high sensitivity to the CP phase. To achieve this, one can use the fact that the effects of NSI, in particular the effects on CP violation, are proportional to the neutrino energy E_ν. To disentangle the genuine CP phase from NSI, one can use two or more experiments with different neutrino energies. The effects of NSI can be as large as $O(1)$ at accelerator neutrino experiments with $E_\nu > 500\,\mathrm{MeV}$ like DUNE. The neutrino spectrum from the MOMENT source peaks around $(200 \sim 300)\,\mathrm{MeV}$ [28], being 10 times smaller than the peak energy at DUNE. Hence, a combination of the future MOMENT and DUNE results could reduce the degeneracy between δ_D and the NSI parameters [40]. Still, the NSI effects at the MOMENT energy are large. Rescaled from the estimation for T2K, the relative correction of NSI to the oscillation probability $P_{\mu e}$ is roughly 10% at MOMENT. For neutrinos from μDAR with energies $\sim (30 - 50)$ MeV the NSI corrections are only 2%.

Various possible experiments with μDAR sources have been explored. In particular, it was proposed [44] to use the Super-K detector (and later Hyper-K) to detect the antineutrino oscillation $\bar{\nu}_\mu \to \bar{\nu}_e$ from μDAR source to Kamioka (dubbed by μKam, which can be either μSK with the Super-K detector or μHK with the Hyper-K detector). The combination of T2K running solely in the neutrino (νT2K) and μSK in the antineutrino mode, referred as TNT2K, provides even higher sensitivity to the CP phase δ_D [44].

In most papers, the NSI effects have been computed numerically although several analytical studies can be found in [6, 45, 46, 35]. These earlier studies provide analytical expressions of the oscillation probabilities in the $\bar{\nu}_e \to \bar{\nu}_e$ [45, 46], $\nu_e \to \nu_\mu$ [6, 46], $\nu_\mu \to \nu_e$ [45, 46, 35], and $\nu_\mu \to \nu_\mu$ [45, 46] channels. In particular, [46] provides the probability formula for all oscillation channels. In this paper, we present an analytical formalism which allows us to analyze the effects of NSI in a simple way. The vacuum mimicking [1] in the 1-2 sector and its violation plays a central role in our formalism. We show that NSI can induce large correction via the violation of vacuum mimicking and apply our results to the CP measurement at TNT2K.

The paper is organized as follows. In Sec. 2 we present a general formalism of matter effects and discuss the role of vacuum mimicking in the sector of 1-2 mass splitting and mixing. We then apply this formalism to the case of standard interactions in Sec. 3 and non-standard interactions in Sec. 4. The vacuum mimicking can be significantly violated by NSI and the Dirac CP phase δ_D can receive $\mathcal{O}(1)$ correction. In Sec. 5 we explore the sensitivity of T2K and μSK experiments to the genuine CP phase in the presence of NSI. Especially, the improvement on the sensitivity due to the μSK component of TNT2K is shown. Our conclusions are given in Sec. 6.

2. Neutrino Oscillation in Matter at Low Energies

2.1. Generalities and physics setup

In the flavor basis, the Hamiltonian $\mathcal{H}$ that describes the neutrino propagation is a sum of the vacuum term and the matrix of matter potential $\mathbb{V}$:

$$\mathcal{H} \equiv \frac{1}{2E_\nu} U_{PMNS} \begin{pmatrix} 0 & & \\ & \Delta m_{21}^2 & \\ & & \Delta m_{31}^2 \end{pmatrix} U_{PMNS}^\dagger + \mathbb{V}, \tag{2.1}$$

---

[1]The effect of vacuum mimicking was noticed in [1, 47, 48], explained in [49], further studied in [50, 51, 52] and dubbed as such in [53].

where $\Delta m_{21}^2 \equiv m_2^2 - m_1^2$, $\Delta m_{31}^2 \equiv m_3^2 - m_1^2$, and E_ν is the neutrino energy. The matrix of matter potential $\mathbb{V}$ in general has contributions from both standard and non-standard interactions. For the mixing matrix in vacuum U_{PMNS} we use the standard parametrization

$$U_{PMNS} \equiv U_{23}(\theta_{23})\Gamma_{\delta_D}U_{13}(\theta_{13})\Gamma_{\delta_D}^\dagger U_{12}(\theta_{12}), \quad \Gamma_{\delta_D} = \mathrm{diag}(1, 1, e^{i\delta_D}).$$

Here θ_{ij} are the vacuum mixing angles and δ_D is the Dirac CP phase. In the case of standard interaction only, the matrix of matter potential takes the form as

$$\mathbb{V} = \mathrm{diag}\{V, 0, 0\} \quad \text{and} \quad V = \sqrt{2}G_F n_e, \tag{2.2}$$

where G_F is the Fermi coupling and n_e is the electron number density. For the standard interaction with a constant density $3\mathrm{g/cm}^3$ of isotopically neutral matter and $\sin^2\theta_{12} \approx 0.31$, the resonance neutrino energy due to the 1-2 mass splitting equals

$$E_R = \cos 2\theta_{12}\frac{\Delta m_{21}^2}{2V} = 122\,\mathrm{MeV}. \tag{2.3}$$

At low energy, $E_\nu \lesssim 1\,\mathrm{GeV}$, the three mass-energy scales $(\Delta m_{21}^2, \Delta m_{31}^2, 2E_\nu V)$ in the Hamiltonian (2.1) satisfy the following conditions:

$$\frac{\Delta m_{21}^2}{2E_\nu} \sim V \ll \frac{\Delta m_{31}^2}{2E_\nu}. \tag{2.4}$$

This allows us to introduce two small parameters

$$r_\Delta \equiv \frac{\Delta m_{21}^2}{\Delta m_{31}^2} \approx 0.03, \quad x_{31} \equiv \frac{2EV}{\Delta m_{31}^2} = 0.01\left(\frac{E_\nu}{100\mathrm{MeV}}\right) \tag{2.5}$$

which will be used for perturbative diagonalization of the Hamiltonian. For typical energies $E_\nu = 50$ MeV at μDAR and $E_\nu = 600$ MeV at T2K, we obtain $x_{31} = 5 \cdot 10^{-3}$ and $x_{31} = 0.06$, respectively.

At low energies the matter corrections to the 1-3 mixing angle and mass splitting are small. It is more convenient to consider the neutrino oscillation in a different basis ν' that is related to the flavor basis ν_f as, [54, 55],

$$\nu_f = \mathcal{R}\nu', \tag{2.6}$$

where

$$\mathcal{R} \equiv U_{23}(\theta_{23})\Gamma_\delta U_{13}(\theta_{13}). \tag{2.7}$$

The matrix $\mathcal{R}$ depends only on the vacuum mixing angles $(\theta_{23}, \theta_{13})$ and the phase δ_D. Using (2.1) and (2.7), we obtain the Hamiltonian in the ν' basis

$$\mathcal{H}' \equiv \mathcal{R}^\dagger\mathcal{H}\mathcal{R} = \frac{\Delta m_{31}^2}{2E_\nu}\begin{bmatrix} 0 & & \\ & 0 & \\ & & 1 \end{bmatrix} + \frac{\Delta m_{21}^2}{2E_\nu}\begin{bmatrix} s_{12}^2 & c_{12}s_{12} & \\ c_{12}s_{12} & c_{12}^2 & \\ & & 0 \end{bmatrix} + \mathbb{V}_{sep}, \tag{2.8}$$

where

$$\mathbb{V}_{sep} \equiv U_{13}^T \Gamma_\delta^\dagger U_{23}^T \mathbb{V} U_{23} \Gamma_\delta U_{13} \,, \tag{2.9}$$

and we use the notation $(c_{ij}, s_{ij}) \equiv (\cos\theta_{ij}, \sin\theta_{ij})$. In this basis, the first term with the largest mass scale Δm_{31}^2 is diagonal and separated from the 1-2 sector in vacuum. The second term in (2.8) depends on the vacuum parameters of the 1-2 sector only while the last term is the matter term that provides all other (in particular 1-3) mixings. For convenience, we call this basis the *separation basis*. It is related to the usual propagation basis [56, 57, 58] by an additional rotation $\Gamma_\delta U_{13}(\theta_{13})$ [54, 55].

Let us introduce a unitary mixing matrix U' to diagonalize the Hamiltonian $\mathcal{H}'$ (2.8):

$$U'^\dagger \mathcal{H}' U' = \mathrm{diag}(H_1, H_2, H_3), \tag{2.10}$$

where H_i are the eigenvalues of $\mathcal{H}'$. Then the total mixing matrix in matter, U^m, which connects the flavor states and the eigenstates of the Hamiltonian $\mathcal{H}$, $\nu_f = U^m \nu^m$, is given by the product

$$U^m = \mathcal{R} U'. \tag{2.11}$$

In (2.11), the vacuum and matter parts are factorized. Without matter effect, we obtain $U' = U_{12}(\theta_{12})$.

In matter with constant density, solving the evolution equation is straightforward. For the eigenstates of the Hamiltonian, ν^m, we obtain according to (2.10) the evolution matrix

$$S^d = \begin{pmatrix} 1 & & \\ & e^{-i\Delta H_{21} L} & \\ & & e^{-i\Delta H_{31} L} \end{pmatrix}, \tag{2.12}$$

where $\Delta H_{ij} \equiv H_i - H_j$ and L is the distance (baseline). Then the matrix of amplitude in the flavor basis is

$$S^f = U^m S^d U^{m\dagger}, \tag{2.13}$$

and the $\nu_\alpha \to \nu_\beta$ ($\alpha, \beta = e, \mu, \tau$) oscillation probability is given by $P_{\alpha\beta} \equiv |S_{\beta\alpha}^f|^2$.

In what follows we will elaborate on the analytical description of the neutrino oscillation effects for the following physics setup:

(i) Neutrino energies are from a few tenths to a few hundreds of MeV.

(ii) The baselines are about half of the oscillation length for the 1-3 mass splitting.

$$L \sim \frac{1}{2} l_{31} = \frac{2\pi E_\nu}{\Delta m_{31}^2}. \tag{2.14}$$

Correspondingly, the (half) oscillation phase equals $\phi_{31} \approx \pi/2$.

(iii) The phase associated with the 2-1 splitting is small:

$$\phi_{21} = r_\Delta \phi_{31} \sim \frac{\pi r_\Delta}{2} \sim 5 \cdot 10^{-2} \quad (\sim 3^\circ). \tag{2.15}$$

Also the matter phase

$$\phi_V = VL \sim \phi_{31} r_\Delta \cos 2\theta_{12} \frac{E_\nu}{E_R} \tag{2.16}$$

is small. The setup is realized in accelerator experiments such as T2(H)K, NOνA, MOMENT, and experiments based on the K-meson, pion and muon decays at rest: KDAR, μDAR, *etc.* [59].

2.2. Oscillation probability

We consider the $\nu_\mu \to \nu_e$ transition in matter. Using (2.12) and (2.13), the probability $P_{\mu e}$ can be generally presented as

$$P_{\mu e} = \left| 2U_{e2}^{m*} U_{\mu 2}^m \sin \phi_{21}^m + 2U_{e3}^{m*} U_{\mu 3}^m \sin \phi_{31}^m e^{-i\phi_{32}^m} \right|^2, \tag{2.17}$$

where $U_{\alpha j}^m$ is the αj-element of the mixing matrix U^m in matter, and the half-oscillation phases equal

$$\phi_{21}^m = \frac{1}{2}\Delta H_{21} L, \quad \phi_{31}^m = \frac{1}{2}\Delta H_{31} L, \quad \phi_{32}^m = \phi_{31}^m - \phi_{21}^m. \tag{2.18}$$

We can rewrite the probability $P_{\mu e}$ using the explicit expressions of $U_{\alpha j}^m$ in the standard parametrization. In particular, the first term in (2.17) becomes

$$2c_{13}^m s_{12}^m \left(c_{12}^m c_{23}^m - s_{13}^m s_{12}^m s_{23}^m e^{i\delta_D^m} \right) \sin \phi_{21}^m, \tag{2.19}$$

where $(c_{ij}^m, s_{ij}^m) \equiv (\cos \theta_{ij}^m, \sin \theta_{ij}^m)$. It is convenient to combine the second term in (2.19) with the second term in (2.17) to get

$$P_{\mu e} \equiv \left| A_{e\mu}^S + A_{e\mu}^A \right|^2. \tag{2.20}$$

Here, we have introduced the "solar" amplitude

$$A_{e\mu}^S = c_{13}^m c_{23}^m A_{12}^m \tag{2.21}$$

with

$$A_{12}^m \equiv \sin 2\theta_{12}^m \sin \phi_{21}^m, \tag{2.22}$$

and the "atmospheric" amplitude

$$A_{e\mu}^A \equiv s_{23}^m \sin 2\theta_{13}^m e^{i\delta_D^m} \left[\sin \phi_{31}^m e^{-i\phi_{32}^m} - s_{12}^{m2} \sin \phi_{21}^m \right]. \tag{2.23}$$

The atmospheric amplitude contains the term with oscillation phase related to the small 2-1 mass splitting and it can be rewritten as

$$A_{e\mu}^A = s_{23}^m A_{13}^m e^{i(\delta_D^m - \phi_{32}^m)} \left[1 - (s_{12}^m)^2 e^{i\phi_{32}^m} \frac{\sin \phi_{21}^m}{\sin \phi_{31}^m} \right], \qquad (2.24)$$

where

$$A_{13}^m \equiv \sin 2\theta_{13}^m \sin \phi_{31}^m. \qquad (2.25)$$

The amplitudes A_{13}^m and A_{12}^m coincide with the standard 2ν oscillation amplitudes.

The 2-1 splitting correction to the atmospheric amplitude (expression in the brackets of (2.24)) can be parametrized as

$$\left[1 - y e^{i\phi_{32}^m} \right] \equiv \kappa e^{-i\phi_\kappa}, \qquad (2.26)$$

where

$$y \equiv s_{12}^{m2} \left(\frac{\sin \phi_{21}^m}{\sin \phi_{31}^m} \right). \qquad (2.27)$$

For the experimental setup under consideration $y \approx s_{12}^{m2} r_\Delta$. Below the 1-2 resonance ($E_\nu < E_R$) we have $s_{12}^{m2} \approx s_{12}^2 = 0.31$, in the resonance $s_{12}^{m2} = 0.5$, and s_{12}^{m2} approaches 1 with E_ν above the resonance. So, typically $y = (1 - 3) \cdot 10^{-2}$ is a small quantity. The quantities in (2.26) equal

$$\kappa = \sqrt{1 - 2y \cos \phi_{32}^m + y^2} \approx 1 - y \cos \phi_{32}^m, \qquad (2.28a)$$

$$\tan \phi_\kappa = \frac{y \sin \phi_{32}^m}{1 - y \cos \phi_{32}^m} \approx y \sin \phi_{32}^m. \qquad (2.28b)$$

Since $y \ll 1$, the phase ϕ_κ is much smaller than ϕ_{32}^m.

Thus, the total probability (2.17) can be written as

$$P_{\mu e} = \left| c_{13}^m c_{23}^m A_{12}^m + s_{23}^m A_{13}^m \kappa e^{i(\delta_D^m - \phi_{32}^m - \phi_\kappa)} \right|^2. \qquad (2.29)$$

Here $\phi_\kappa = \phi_\kappa(\phi_{32}^m)$ is small correction to the oscillation phase ϕ_{32}^m. If $\kappa = 1$, Eq. (2.32) reproduces the standard expression for $P_{\mu e}$.

In the case of standard interactions, the vacuum mimicking for the 1-2 amplitude is realized due to smallness of the 2-1 phase $\phi_{21}^m \ll 1$, [1, 47, 48, 49, 50, 51, 52, 53]

$$A_{12}^m \equiv \sin 2\theta_{12}^m \sin \phi_{21}^m \approx \sin 2\theta_{12} \sin \phi_{21} = A_{12}, \qquad (2.30)$$

For $\phi_{21}^m \ll 1$, (2.30) gives $A_{12}^m \simeq \sin 2\theta_{12} \frac{\Delta m_{21}^2 L}{2E_\nu}$. The condition $\phi_{21}^m \ll 1$ for vacuum mimicking is fulfilled in the majority of existing and proposed experiments.

In general, vacuum mimicking is broken in the presence of NSI [49]. Introducing parameter

$$r_V \equiv \frac{A_{12}^m}{A_{12}} \qquad (2.31)$$

to quantify the deviation from vacuum mimicking, we can rewrite the ptobability $P_{\mu e}$ as

$$P_{\mu e} \approx \left| c_{13}^m c_{23}^m r_V A_{12} + s_{23}^m A_{13}^m \kappa e^{i(\delta_D^m - \phi_{32}^m - \phi_\kappa)} \right|^2 . \tag{2.32}$$

This parametrization of the probability $P_{\mu e}$ is convenient for understanding the matter effects, including both standard and non-standard interactions.

The probability $P_{\mu e}$ in (2.32) can also be rewritten as sum of the atmospheric, solar and interference terms:

$$P_{\mu e} \approx P_{\mu e}^A + P_{\mu e}^S + P_{\mu e}^I \cos \left(\delta_D^m - \phi_{32}^m - \phi_\kappa \right) . \tag{2.33}$$

Here

$$P_{\mu e}^A = |A_{\mu e}^A|^2 \equiv \kappa^2 s_{23}^{m2} \sin^2 2\theta_{13}^m \sin^2 \phi_{31}^m , \tag{2.34}$$

$$P_{\mu e}^S = |A_{\mu e}^S|^2 \approx r_V^2 c_{23}^{m2} c_{13}^{m2} \sin^2 2\theta_{12} \sin^2 \phi_{21} , \tag{2.35}$$

$$P_{\mu e}^I \equiv \kappa r_V \sin 2\theta_{23}^m c_{13}^m \sin 2\theta_{13}^m \sin \phi_{31}^m \sin 2\theta_{12} \sin \phi_{21} . \tag{2.36}$$

For constant density, the problem then reduces to finding the mixing angles and mass splittings in matter. The exact vacuum mimicking corresponds to $r_V = 1$. If in addition $\kappa = 1$ and $\phi_\kappa = 0$, Eqs.(2.33-2.36) reproduce the usual approximate expression for $P_{\mu e}$ [60].

It is easy to see that the 1-2 correction to the atmospheric amplitude

$$\kappa - 1 \propto \sin^2 \theta_{12}^m \sin \phi_{21}^m = A \frac{\Delta m_{21}^2 L}{4 E_\nu} \tag{2.37}$$

does not show vacuum mimicking and has strong dependence on the matter potential V. For $V \to 0$: $A \to \sin^2 \theta_{12}$, in the resonance $A \to \sin 2\theta_{12}$ and with further increase of V the coefficient A increases as $\propto V$.

2.3. On vacuum mimicking

Let us present vacuum mimicking in a general form for both standard and non-standard interactions. Consider for simplicity the 2ν Hamiltonian with moduli of the off-diagonal elements $|\bar{\mathcal{H}}|$ and difference of the eigenvalues $\Delta \mathcal{H}$. The mixing angle is given by

$$\sin 2\theta_{12}^m = \frac{2|\bar{\mathcal{H}}|}{\Delta \mathcal{H}}, \tag{2.38}$$

and the (half) oscillation phase equals

$$\phi_{21}^m = \frac{1}{2} \Delta \mathcal{H} L. \tag{2.39}$$

Then

$$A_{21}^m \approx \sin 2\theta_{12}^m \; \phi_{21}^m = \frac{2|\bar{\mathcal{H}}|}{\Delta\mathcal{H}} \frac{1}{2}\Delta\mathcal{H}L = |\bar{\mathcal{H}}|L. \tag{2.40}$$

So, the oscillation amplitude A_{21}^m in the first order is given by the off-diagonal element of the 2ν Hamiltonian multiplied by distance. Since for standard interaction the matter potential appears only in the diagonal elements of the Hamiltonian in the flavor basis, $\bar{\mathcal{H}} = \bar{\mathcal{H}}_V$, we obtain $A_{21}^m = A_{21}$. The deviation from vacuum mimicking appears when the off-diagonal element $\bar{\mathcal{H}}$ depends on matter potential.

Even for the standard interactions, matter effect appears in A_{12}^m when $\sin \phi_{21}^m$ is expanded to higher order,

$$A_{12}^m \equiv \sin 2\theta_{12} \frac{\Delta m_{21}^2 L}{2E_\nu} \left[1 - \frac{1}{6}\left(\frac{\Delta H_{21} L}{2}\right)^2 \right]. \tag{2.41}$$

For the vacuum amplitude A_{12} we have the same expression with substitution $\Delta H_{21} \to \Delta m_{21}^2 / 2E_\nu$. Then the ratio of the matter to vacuum amplitudes equals

$$r_V = 1 + \frac{1}{3}(\phi_{21})^2 \cos^2 2\theta_{12} c_{13}^2 \left(1 - \frac{c_{13}^2}{2}\frac{E}{E_R} \right). \tag{2.42}$$

Using (2.15) we can estimate the matter corrections as

$$r_V - 1 \approx \frac{1}{3}\left(\frac{\pi r_\Delta}{2}\right)^2 \cos^2 2\theta_{12} \left(1 - \frac{E}{2E_R} \right) \approx 10^{-4}. \tag{2.43}$$

According to (2.43), tn addition to the small oscillation phase squared, the correction $r_V - 1$ is suppressed by $\cos^2 2\theta_{12}/3 \approx 0.03$. Note that $r_V - 1$ is positive for neutrinos because $\Delta H_{21} < \Delta m_{21}^2 / 2E_\nu$ and increases with energy. For antineutrinos it is negative.

One comment is in order. Recently there was a discussion on why the formulas for the 3ν-oscillation probabilities in matter derived for $E \gg E_{21}^R$ (i.e., far above the 1-2 resonance) work well at $E \sim E_{21}^R$ [61]. Rather complicated explanation has been proposed in [62]. In fact, the reason is simple. For small values of the 2-1 phase, which is true at all proposed long-baseline experiments, the vacuum mimicking is realized. In spite of large matter corrections to the oscillation phase and mixing angle, the corrections cancel with each other in the oscillation probabilities. The same expression for the oscillation probability applies at all energies as long as the matter phase is small and the presence of the 1-2 resonance or not is irrelevant.

Corrections due to κ (2.28a) and (2.37) depend on the 1-2 sector parameters, $\kappa = \kappa(\theta_{21}, \Delta_{21}, V)$, and break vacuum breaking. In the 3ν case the vacuum mimicking does not work exactly even for the standard interaction. As can be seen from (2.33) the matter effect associated with the 1-2 splitting, ϕ_{21}^m, appears in the phase of the interference term. To realize the vacuum mimicking, one needs to

reduce 3ν evolution to 2ν evolution associated with small mass splitting. In the 3ν case, the violation of vacuum mimicking can be induced even by the diagonal elements of the matter potential matrix (see below).

3. Standard Interaction and Vacuum Mimicking

3.1. Oscillation parameters

Using the expression (2.2) of $\mathbb{V}$ for the standard interactions in the flavor basis, we obtain the matrix of matter potential in the separation basis,

$$\mathbb{V}_{sep} = U_{13}^T \mathbb{V} U_{13} = V \begin{pmatrix} c_{13}^2 & & c_{13}s_{13} \\ & 0 & \\ c_{13}s_{13} & & s_{13}^2 \end{pmatrix}. \tag{3.1}$$

Consequently, the total Hamiltonian (2.8) can be written explicitly as

$$\mathcal{H}' = \frac{\Delta m_{31}^2}{2E_\nu} \begin{pmatrix} 0 & & \\ & 0 & \\ & & 1 \end{pmatrix} + \frac{\Delta m_{21}^2}{2E_\nu} \begin{pmatrix} s_{12}^2 & c_{12}s_{12} & \\ c_{12}s_{12} & c_{12}^2 & \\ & & 0 \end{pmatrix} + V \begin{pmatrix} c_{13}^2 & & c_{13}s_{13} \\ & 0 & \\ c_{13}s_{13} & & s_{13}^2 \end{pmatrix}. \tag{3.2}$$

Here the 1-3 mixing (being proportional to θ_{13}) is generated by matter potential.

An additional 1-3 rotation

$$\delta\theta_{13} \approx \tan\delta\theta_{13} \approx s_{13}c_{13}\frac{2E_\nu V}{\Delta m_{31}^2} = s_{13}c_{13}x_{31} \tag{3.3}$$

eliminates the 1-3 and 3-1 elements of the Hamiltonian (3.2). This rotation, in turn, generates non-zero 2-3 and 3-2 elements which have next order of smallness and can be neglected. Consequently, $\theta_{23}^m \approx \theta_{23}$ (see [55] for details).

After the rotation (3.3) the third state decouples and for the rest of the system we obtain the effective 2ν Hamiltonian

$$\mathcal{H}'_{2\nu} \approx \frac{\Delta m_{21}^2}{2E_\nu} \begin{pmatrix} s_{12}^2 + c_{13}^2 x_{21} & c_{12}s_{12} \\ c_{12}s_{12} & c_{12}^2 \end{pmatrix}, \tag{3.4}$$

where

$$x_{21} \equiv \frac{2E_\nu V}{\Delta m_{21}^2} = 0.28 \left(\frac{E_\nu}{100 \text{ MeV}} \right). \tag{3.5}$$

For typical energies of μDAR and T2K, we have $x_{21} = 0.14$ and $x_{21} = 1.5$. The correction to the 1-1 element generated by decoupling is of the order $r_\Delta s_{13}^2$, and therefore has been neglected in (3.4).

Notice that the Hamiltonian (3.4) can be obtained by block-diagonalization (3.2) and decoupling of the third state.

The diagonalization of (3.4) gives the effective mass splitting

$$\Delta H_{21} = \frac{\Delta m_{21}^2}{2E} \sqrt{\sin^2 2\theta_{12} + (\cos 2\theta_{12} - c_{13}^2 x_{21})^2}, \tag{3.6}$$

and the 1-2 mixing angle in matter

$$\sin 2\theta_{12}^m = \frac{\Delta m_{21}^2}{2E\Delta H_{21}} \sin 2\theta_{12}. \tag{3.7}$$

The 1-3 splitting (upper sign) and the 2-3 spitting (lower sign) are

$$\Delta H_{31}(\Delta H_{32}) \approx \frac{\Delta m_{31}^2}{2E} - \frac{1}{2}\left[\frac{\Delta m_{21}^2}{2E} \mp \Delta H_{21} + (c_{13}^2 - 2s_{13}^2)V\right]. \tag{3.8}$$

Thus, the diagonalization matrix in the separation basis is given by

$$U' = U_{13}(\delta\theta_{13})U_{12}(\theta_{12}^m), \tag{3.9}$$

and the total mixing matrix in matter becomes

$$U^m = \mathcal{R}U' = U_{23}(\theta_{23})\Gamma_{\delta_D}U_{13}(\theta_{13}^m)U_{12}(\theta_{12}^m), \tag{3.10}$$

where

$$\theta_{13}^m = \theta_{13} + \delta\theta_{13}. \tag{3.11}$$

The matter correction to the CP phase is absent: $\delta_D^m = \delta_D$.

3.2. The oscillation probability

The probability of $\nu_\mu \to \nu_e$ transition is given in (2.33 - 2.36). Taking $r_V \approx 1$, $c_{23}^m \approx c_{23}$, $s_{23}^m \approx s_{23}$ and $\delta_D^m = \delta_D$, it becomes

$$\begin{aligned} P_{\mu e} &= \kappa^2 s_{23}^2 \sin^2 2\theta_{13}^m \sin^2 \phi_{31}^m + c_{23}^2 c_{13}^{m2} \sin^2 2\theta_{12} \sin^2 \phi_{21} \\ &+ \kappa \sin 2\theta_{23} c_{13}^m \sin 2\theta_{13}^m \sin \phi_{31}^m \sin 2\theta_{12} \sin \phi_{21} \cos(\delta_D - \phi_{32}^m - \phi_\kappa). \end{aligned} \tag{3.12}$$

The correction to the atmospheric amplitude given by $(\kappa - 1) \sim r_\Delta$ can also be neglected. Then for $\kappa = 1$ and $\phi_\kappa = 0$, (3.12) reproduces the commonly used formula of $P_{\mu e}$ [60]. The oscillation parameters in matter θ_{13}^m, ϕ_{31}^m, and ϕ_{32}^m that enter this formula have been obtained in Eqs. (3.6), (3.7), (3.8), (3.11).

In Fig. 1 (left panel) we show the dependence of the probability $P_{\mu e}$ on E_ν/L for the T2K setup and different values of δ_D. At the first oscillation maximum, $E_\nu/L \approx 1.8$, we have $P_{\mu e}(0) = P_{\mu e}(\pi)$ and

$P_{\mu e}(\pm\pi/2) = (1 \pm 1/3)P_{\mu e}(0)$ where the minus sign corresponds to the presently favored $\delta_D = 3\pi/2$. The spread of the values of $P_{\mu e}(\delta_D)$ with varying δ_D is more than 60%.

According to (2.36) $P_{\mu e}^A \propto s_{13}^2$, $P_{\mu e}^S$ is suppressed by $\sin^2\phi_{21} \propto r_\Delta^2$, and $P_{\mu e}^I \propto s_{13}r_\Delta$. So, the following hierarchy

$$\frac{P_{\mu e}^S}{P_{\mu e}^A} \approx \sin^2 2\theta_{12}\frac{\phi_{21}^2}{4s_{13}^2} \approx \frac{2}{9}\left(\frac{\pi r_\Delta}{2s_{13}}\right)^2 \approx 2\%, \tag{3.13a}$$

$$\frac{P_{\mu e}^I}{P_{\mu e}^A} \approx \frac{\sin 2\theta_{12}}{s_{13}}\phi_{21} \approx \frac{\pi r_\Delta}{2s_{13}} \approx 30\%, \tag{3.13b}$$

is realized between the three components at the first oscillation maximum. Roughly, $P_{\mu e}^A : P_{\mu e}^I : P_{\mu e}^S = 50 : 15 : 1$ which holds also above the resonance (see Fig. 1) but changes significantly with decrease of energy: at $E_\nu/L \approx 1.2$ we have $P_{\mu e}^A = P_{\mu e}^I$ and $P_{\mu e}^S = P_{\mu e}^A/4$. Similar relations between the different components of $P_{\mu e}$ are also realized at μSK.
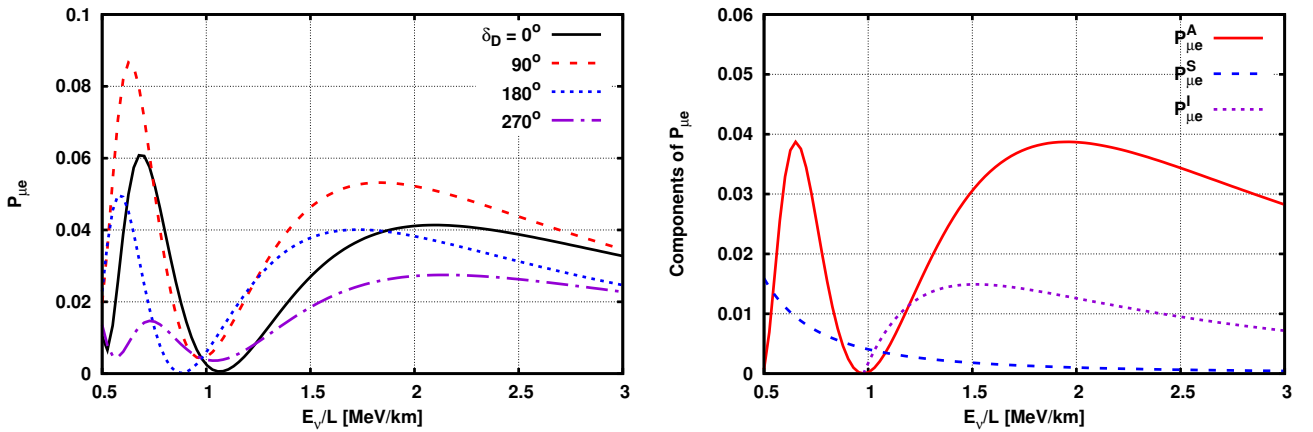

Fig. 1: The oscillation probability $P_{\mu e}$ as a function of E_ν/L for different values of the CP phase δ_D (left). Different components of $P_{\mu e}$ ($P_{\mu e}^A$, $P_{\mu e}^I$, $P_{\mu e}^S$) as functions of E_ν/L for $\delta_{CP} = 3\pi/2$. We use the T2(H)K baseline $L = 295$ km.

The matter correction to the whole oscillation probability $P_{\mu e}$ mainly comes from the angle θ_{13}^m and the phase ϕ_{31}^m. Using $P_{\mu e}^A$ only we find

$$V\frac{\partial P_{\mu e}^A}{\partial V} \approx \frac{1}{2}s_{23}^2\sin^2 2\theta_{13}\sin\phi_{31}\left[4\sin\phi_{31}\frac{2E_\nu V}{\Delta m_{31}^2} - c_{13}^2\cos\phi_{31}VL\right]$$

$$\approx s_{23}^2\sin^2 2\theta_{13}\sin^2\phi_{31}\frac{4E_\nu V}{\Delta m_{31}^2}\left[1 - c_{13}^2\cot\phi_{31}\frac{\phi_{31}}{2}\right]$$

$$\approx \sin^2 2\theta_{13}x_{31}(1 - 0.5c_{13}^2\phi_{31}\cot\phi_{31}). \tag{3.14}$$

The first term in (3.14) comes from θ_{13}^m while the second from ϕ_{31}^m. At the first oscillation maximum, the second term is suppressed by $\cot\phi_{31} \approx 0$. However, if the neutrino energy spectrum is wide enough, $\cos\phi_{31}$ can become sizable out of the peak, as shown in Fig. 2. According to Fig. 2, $P_{\mu e}$ and $P_{\mu e}^I$ at T2K and μSK are very similar when expressed as functions of E_ν/L. At the first oscillation

maximum $P_{\mu e}^I/P_{\mu e} \approx 0.3$ and the matter effect increases with energy as

$$P_{\mu e} - P_{\mu e}^{vac} \propto E_\nu$$

according to (3.14). Therefore the matter effect at μSK is typically 12 times smaller than at T2K. With respect to the interference (CP) term, the matter effect is about $(25 - 30)\%$ at T2K and $(2.0 - 2.2)\%$ at μSK.
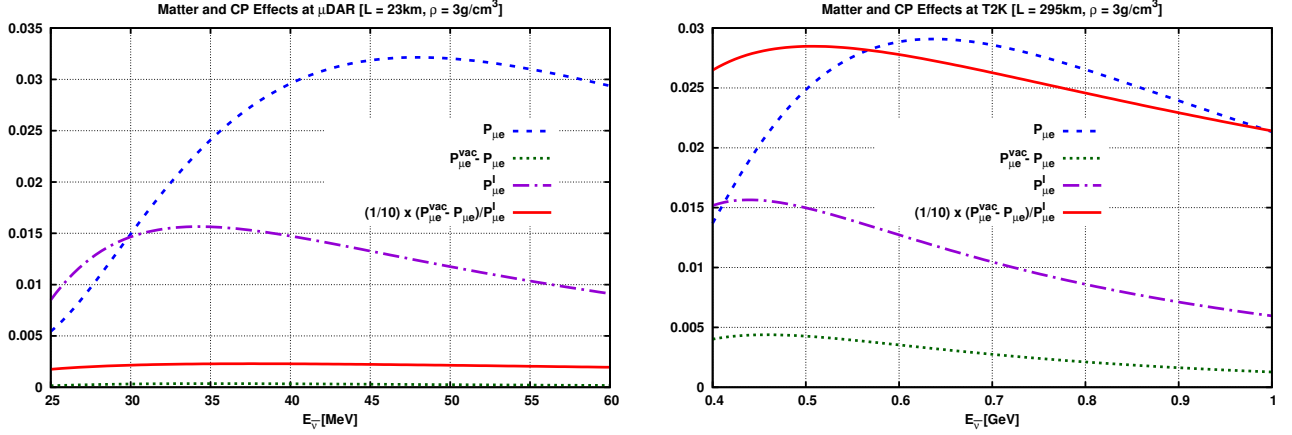

Fig. 2: The matter effect on probabilities $(P_{\mu e}^{vac} - P_{\mu e})$ and the CP term coefficient $P_{\mu e}^I$ at μDAR (left) and T2(H)K (right) for $\delta_D = 3\pi/2$.

For standard interactions, the matter corrections mainly come from the 1-3 mixing s_{13}^m, being $\sim 13\%$ at T2K and $\sim 1\%$ at μDAR, at the first oscillation peak and for $\delta_D = 3\pi/2$. The matter effect from the 1-2 sector is strongly suppressed by the vacuum mimicking, producing $\mathcal{O}(r_\Delta)$ correction to the atmospheric amplitude $A_{\mu e}^A$. The interference term is about $1/3$ of the total probability.

4. Effects of Non-Standard Interactions

4.1. Oscillation parameters in the presence of NSI

In the presence of NSI, the matter potential matrix $\mathbb{V}$ in the flavor basis can be parametrized as

$$\mathbb{V} = \begin{pmatrix} V & & \\ & 0 & \\ & & 0 \end{pmatrix} + V \begin{pmatrix} \epsilon_{ee} & \epsilon_{e\mu} & \epsilon_{e\tau} \\ \epsilon_{e\mu}^* & \epsilon_{\mu\mu} & \epsilon_{\mu\tau} \\ \epsilon_{e\tau}^* & \epsilon_{\mu\tau}^* & \epsilon_{\tau\tau} \end{pmatrix} . \tag{4.1}$$

(We do not separate here scattering on different components of matter: electrons, u- and d- quarks, summing up the effect.) The 1σ constraints on the NSI parameters $\epsilon_{\alpha\beta}$ from the global fit [63] are

$$|\epsilon_{e\mu}| < 0.16, \qquad |\epsilon_{e\tau}| < 0.26, \qquad |\epsilon_{\mu\tau}| < 0.02, \tag{4.2a}$$

$$-0.018 < \epsilon_{\tau\tau} - \epsilon_{\mu\mu} < 0.054, \qquad 0 < \epsilon_{ee} - \epsilon_{\mu\mu} < 0.93. \tag{4.2b}$$

The hierarchy among these constraints can be described by powers of small parameter $\lambda = 0.15$ (notice that $s_{13} \approx \lambda$):

$$\epsilon_{ee} - \epsilon_{\mu\mu} < \mathcal{O}(1), \qquad \epsilon_{e\mu}, \ \epsilon_{e\tau} < \mathcal{O}(\lambda), \qquad \epsilon_{\mu\tau}, \ \epsilon_{\tau\tau} - \epsilon_{\mu\mu} < \mathcal{O}(\lambda^2). \tag{4.3}$$

Consequently, the matrix of matter potential in the flavor basis can have the maximal allowed 1σ values,

$$\mathbb{V} \sim V \begin{pmatrix} 1 & \lambda & \lambda \\ \lambda & \lambda^2 & \lambda^2 \\ \lambda & \lambda^2 & \lambda^2 \end{pmatrix}. \tag{4.4}$$

In the separation basis, the matrix of matter potentials is given by transformation of (4.1):

$$\mathbb{V}_{sep} = U_{13}^T \Gamma_\delta^\dagger U_{23}^T \mathbb{V} U_{23} \Gamma_\delta U_{13} = V \begin{pmatrix} \epsilon'_{11} + c_{13}^2 & \epsilon'_{12} & \epsilon'_{13} + s_{13}c_{13} \\ \epsilon'^*_{12} & \epsilon'_{22} & \epsilon'_{23} \\ \epsilon'^*_{13} + s_{13}c_{13} & \epsilon'^*_{23} & \epsilon'_{33} + s_{13}^2 \end{pmatrix}, \tag{4.5}$$

where

$$
\begin{aligned}
\epsilon'_{11} &= c_{13}^2(\epsilon_{ee} - \epsilon_{\mu\mu}) + s_{13}^2\left[c_{23}^2(\epsilon_{\tau\tau} - \epsilon_{\mu\mu}) + 2c_{23}s_{23}\mathbb{R}(\epsilon_{\mu\tau})\right] - 2c_{13}s_{13}\mathbb{R}\left[(s_{23}\epsilon_{e\mu} + c_{23}\epsilon_{e\tau})e^{i\delta_D}\right], \\
\epsilon'_{12} &= c_{13}(c_{23}\epsilon_{e\mu} - s_{23}\epsilon_{e\tau}) + s_{13}e^{-i\delta_D}\left[c_{23}s_{23}(\epsilon_{\tau\tau} - \epsilon_{\mu\mu}) - (\cos 2\theta_{23}\mathbb{R} - i\mathbb{I})(\epsilon_{\mu\tau})\right], \\
\epsilon'_{13} &= c_{13}s_{13}\left[(\epsilon_{ee} - \epsilon_{\mu\mu}) - c_{23}^2(\epsilon_{\tau\tau} - \epsilon_{\mu\mu}) - 2c_{23}s_{23}\mathbb{R}(\epsilon_{\mu\tau})\right] + (\cos 2\theta_{13}\mathbb{R} + i\mathbb{I})\left[(s_{23}\epsilon_{e\mu} + c_{23}\epsilon_{e\tau})e^{i\delta_D}\right], \\
\epsilon'_{22} &= -2c_{23}s_{23}\mathbb{R}(\epsilon_{\mu\tau}) + s_{23}^2(\epsilon_{\tau\tau} - \epsilon_{\mu\mu}), \\
\epsilon'_{23} &= s_{13}(c_{23}\epsilon^*_{e\mu} - s_{23}\epsilon^*_{e\tau}) - c_{13}e^{i\delta_D}\left[c_{23}s_{23}(\epsilon_{\tau\tau} - \epsilon_{\mu\mu}) - (\cos 2\theta_{23}\mathbb{R} + i\mathbb{I})(\epsilon_{\mu\tau})\right], \\
\epsilon'_{33} &= s_{13}^2(\epsilon_{ee} - \epsilon_{\mu\mu}) + c_{13}^2\left[c_{23}^2(\epsilon_{\tau\tau} - \epsilon_{\mu\mu}) + 2c_{23}s_{23}\mathbb{R}(\epsilon_{\mu\tau})\right] + 2c_{13}s_{13}\mathbb{R}\left[(s_{23}\epsilon_{e\mu} + c_{23}\epsilon_{e\tau})e^{i\delta_D}\right].
\end{aligned} \tag{4.6}
$$

The operators $\mathbb{R}$ and $\mathbb{I}$ extract the real and imaginary parts from the attached quantities, e.g. $\mathbb{R}(\epsilon_{\mu\tau}) \equiv \mathrm{Re}(\epsilon_{\mu\tau})$. For convenience, we have subtracted from $\mathbb{V}$ a diagonal term $\epsilon_{\mu\mu}$ proportional to the unit matrix $\mathbb{I}_{3\times3}$ which does not affect oscillation probabilities. Notice that the elements of $\mathbb{V}_{sep}$ in the separation basis have the same hierarchy of values as (4.4) in the flavor basis due to hierarchical values of the mixing angles $s_{13} = \mathcal{O}(\lambda)$ and $s_{23} = \mathcal{O}(1)$ in (4.5).

We can diagonalize the total Hamiltonian in the same way as in the case of standard interaction. First, block-diagonalization gives the effective 2ν Hamiltonian

$$\mathcal{H}'_{2\nu} \approx \frac{\Delta m_{21}^2}{2E_\nu} \begin{pmatrix} s_{12}^2 + x_{21}(c_{13}^2 + \epsilon'_{11}) & s_{12}c_{12} + x_{21}\epsilon'_{12} \\ s_{12}c_{12} + x_{21}\epsilon'^*_{12} & c_{12}^2 + x_{21}\epsilon'_{22} \end{pmatrix} \tag{4.7}$$

for the first two states. The decoupled state has the eigenvalue

$$H_3 \approx \frac{\Delta m_{31}^2}{2E} + V(s_{13}^2 + \epsilon'_{33}). \tag{4.8}$$

14

In the first approximation, this block-diagonalization is equivalent to an additional 1-3 rotation

$$\Gamma_{\delta_3} U_{13}(\delta\theta_{13})$$

which removes the 1-3 and 3-1 elements of the total Hamiltonian. Here

$$\Gamma_{\delta_3} \equiv diag(1, 1, e^{i\delta_3}), \quad \delta_3 = \text{Arg}[s_{13}c_{13} + \epsilon'_{13}], \tag{4.9}$$

and the rotation angle in $U_{13}(\delta\theta_{13})$ is determined approximately by

$$\delta\theta_{13} \approx \tan\delta\theta_{13} \approx x_{31}\frac{|s_{13}c_{13} + \epsilon'_{13}|}{1 + x_{31}(s_{13}^2 + \epsilon'_{33})} \approx x_{31}|s_{13}c_{13} + \epsilon'_{13}|. \tag{4.10}$$

Numerically, $\delta\theta_{13} \sim \mathcal{O}(\lambda^3)$, but the phase δ_3 can be large, $\delta_3 = \mathcal{O}(1)$, since $\epsilon'_{13} \sim s_{13} \sim \lambda$.

In this approximation, we have neglected the 2-3 and 3-2 elements of the Hamiltonian. They can be eliminated by an additional 2-3 rotation on the angle

$$\delta\theta_{23} \approx x_{31}|\epsilon'_{23}| \tag{4.11}$$

which has the next order of smallness: $\delta\theta_{23} = \mathcal{O}(\lambda^4)$.

Diagonalization of the matrix (4.7) gives the effective mass splitting

$$\Delta H_{21} = \frac{\Delta m_{21}^2}{2E}\sqrt{[\cos 2\theta_{12} - x_{21}(c_{13}^2 + \epsilon'_{11} - \epsilon'_{22})]^2 + (\sin 2\theta_{12} + 2x_{21}\epsilon'_{12})^2}, \tag{4.12}$$

and mixing $\Gamma_{\delta_2} U_{12}(\theta_{12}^m)$ where

$$\sin 2\theta_{12}^m = \frac{\Delta m_{21}^2}{2E\Delta H_{21}}|\sin 2\theta_{12} + 2x_{21}\epsilon'_{12}|, \tag{4.13}$$

$$\Gamma_{\delta_2} = diag(1, e^{i\delta_2}), \quad \delta_2 = -\text{Arg}[\sin 2\theta_{12} + 2x_{21}\epsilon'_{12}]. \tag{4.14}$$

Notice that with NSI the off-diagonal element of the Hamiltonian $\mathcal{H}'_{2\nu}$ are complex and so additional rephasing Γ_{δ_2} is needed. In fact, the phase δ_2 also originates from the violation of vacuum mimicking, being the phase of the off-diagonal element $\mathcal{H}_{12}$ (or equivalently $\bar{\mathcal{H}}$ in (2.38) for the 2ν Hamiltonian).

Using the trace of the Hamiltonian (4.7) as well as the equalities (4.8) and (4.12), we find the 1-3 mass splitting

$$\Delta H_{31} \approx \frac{\Delta m_{31}^2}{2E} + V(s_{13}^2 + \epsilon'_{33}) - \frac{1}{2}\left[\frac{\Delta m_{21}^2}{2E} - \Delta H_{21} + (c_{13}^2 + \epsilon'_{11} + \epsilon'_{22})V\right]. \tag{4.15}$$

Combining all the rotations we obtain the total mixing matrix in matter

$$U_m = \mathcal{R}U' = U_{23}(\theta_{23})\Gamma_{\delta_D}U_{13}(\theta_{13})\Gamma_{\delta_3}U_{13}(\delta\theta_{13})\Gamma_{\delta_2}U_{12}(\theta_{12}^m). \tag{4.16}$$

Notice that if $\delta_3 = 0$, the correction $\delta\theta_{13}$ can be combined with θ_{13} as in the standard interaction case (3.11).

To find the effective mixing angles in matter, the matrix (4.16) should be reduced to the standard parametrization. Since Γ_{δ_2} commutes with the 1-3 rotations on the left-hand side, it can be combined with Γ_{δ_D}:

$$\Gamma_{\delta_D}\Gamma_{\delta_2} = \text{diag}\left[1, e^{i\delta_2}, e^{i\delta_2}\right]\text{diag}\left[1, 1, e^{i(\delta_D-\delta_2)}\right]. \tag{4.17}$$

The first matrix in (4.17) can be omitted since it commutes with the 2-3 rotations in (4.16), and therefore can be absorbed in the rephasing of the charged lepton states.

It is straightforward to show that the product of the 1-3 transformations $U_{13}(\theta_{13})\Gamma_{\delta_3}U_{13}(\delta\theta_{13})$ can be written as

$$U_{13}(\theta_{13})\Gamma_{\delta_3}U_{13}(\delta\theta_{13}) = \Gamma_3\Gamma_C\Gamma_\alpha U_{13}(\theta_{13}^m)\Gamma_\beta. \tag{4.18}$$

Here

$$\Gamma_3 = \text{diag}\left(e^{i\delta_3/2}, 1, e^{i\delta_3/2}\right), \tag{4.19}$$

$$\Gamma_C = \text{diag}\left(e^{i\phi_C}, 1, e^{i\phi_C}\right), \tag{4.20}$$

$$\Gamma_\alpha = \text{diag}\left(1, 1, e^{-i(\phi_S+\phi_C)}\right), \tag{4.21}$$

$$\Gamma_\beta = \text{diag}\left(1, 1, e^{i(\phi_S-\phi_C)}\right), \tag{4.22}$$

and the phase ϕ_S is determined from

$$\tan\phi_S = \tan\left(\frac{\delta_3}{2}\right)\frac{\sin(\theta_{13}-\delta\theta_{13})}{\sin(\theta_{13}+\delta\theta_{13})}, \tag{4.23}$$

and the phase ϕ_C has similar expression with substitution $\sin \to \cos$ and overall minus sign. Then, the 1-3 mixing angle in matter is given by

$$\cos\theta_{13}^m = \sqrt{\cos^2(\delta_3/2)\cos^2(\theta_{13}+\delta\theta_{13}) + \sin^2(\delta_3/2)\cos^2(\theta_{13}-\delta\theta_{13})}. \tag{4.24}$$

After inserting (4.18) into (4.16), we find a number of simplifications. The matrix Γ_β commutes with the 1-2 rotation and therefore can be absorbed into the rephasing of the eigenstates of the Hamiltonian. The product $\Gamma_3\Gamma_C\Gamma_\alpha$ can be written as

$$\Gamma_3\Gamma_C\Gamma_\alpha = \text{diag}\left[e^{i(\delta_3/2+\phi_C)}, 1, 1\right] \times \text{diag}\left[1, 1, e^{i(\delta_3/2-\phi_S)}\right]. \tag{4.25}$$

The first matrix commutes with the 2-3 rotation of (4.16) and therefore can be absorbed into the rephasing of the flavor states. The second matrix can be combined with the matrix in (4.17). As a result, we obtain the standard expression for the mixing matrix

$$U_m = \mathcal{R}U' = U_{23}(\theta_{23})\Gamma_{\delta_D^m}U_{13}(\theta_{13}^m)U_{12}(\theta_{12}^m) \tag{4.26}$$

with

$$\Gamma_{\delta_D^m} = (1, 1, e^{i\delta_D^m}), \qquad \delta_D^m \equiv \delta_D - \delta_2 + \frac{\delta_3}{2} - \phi_S. \tag{4.27}$$

Here δ_D^m is the effective CP phase in matter which includes corrections from NSI.

The obtained expressions for the effective mixing parameters in matter can be simplified using the smallness of $\delta\theta_{13}$ (4.10). From (4.23) we find

$$\frac{\delta_3}{2} - \phi_S \approx x_{31}c_{13}^2 \left| 1 + \frac{\epsilon_{13}'}{c_{13}s_{13}} \right| \sin\delta_3 \, , \tag{4.28}$$

so that the effective CP phase in matter becomes

$$\delta_D^m \approx \delta_D - \delta_2 + x_{31}c_{13}^2 \left| 1 + \frac{\epsilon_{13}'}{c_{13}s_{13}} \right| \sin\delta_3 \, . \tag{4.29}$$

For the effective 1-3 mixing angle in matter we have

$$\theta_{13}^m \approx \theta_{13} + \cos\delta_3\delta\theta_{13}. \tag{4.30}$$

Recall that $\delta_2 = \delta_2(\epsilon_{12}')$ is a function of ϵ_{12}', whereas $\delta_3 = \delta_3(\epsilon_{13}')$ is a function of ϵ_{13}'.

According to our consideration here, the matter potential (including NSI) influences the mixing angles, the CP phase, and the splittings of the eigenvalues of the Hamiltonian in rather specific ways which we will discuss in the next two subsections.

4.2. Matter corrections and the violation of vacuum mimicking

The matter potential influences the 1-2 mixing and splitting in a particular form that can be described with high accuracy as the violation of vacuum mimicking. The non-diagonal element of the Hamiltonian (4.7),

$$\mathcal{H}'_{12} = s_{12}c_{12} + x_{21}\epsilon_{12}', \tag{4.31}$$

depends on the NSI parameter ϵ_{12}' and therefore vacuum mimicking is broken [49] already at the lowest order, according to the discussions related to (2.40). The violation of vacuum mimicking is characterized by

$$r_V = \frac{|\mathcal{H}'_{12}|}{\mathcal{H}_{12}} = \left| 1 + \frac{2x_{21}\epsilon_{12}'^*}{\sin 2\theta_{12}} \right| = |1 + \xi_{21}\epsilon_{12}'^*| \, , \tag{4.32}$$

where we have denoted

$$\xi_{21} \equiv \frac{2x_{21}}{\sin 2\theta_{12}}. \tag{4.33}$$

For T2K peak energy, $E_\nu \sim 600$ MeV, the deviation $r_V - 1 \approx 2.30\epsilon_{12}'$ can be as large as $\mathcal{O}(1)$. For μDAR ($E_\nu = 50$ MeV) we have $(r_V - 1) \sim 0.215\,\epsilon_{12}'$. Here the deviation also scales linearly with energy. Consequently, the deviation at T2K is about 12 times larger than the one at μDAR.

The violation parameter r_V (2.31) of vacuum mimicking equals

$$r_V = \sqrt{1 + 2\xi_{21}|\epsilon_{12}'|\cos\phi_\epsilon + \xi_{21}^2|\epsilon_{12}'|^2} \tag{4.34}$$

with $\phi_\epsilon \equiv \mathrm{Arg}[\epsilon'_{12}]$.

There are two effects of the violation of vacuum mimicking:

1. Being attached to the solar amplitude (2.31), the phase factor $e^{i\delta_2}$ contributes to the phase of the interference term (2.33) directly:

$$\delta_D - \delta_2 - \phi^m_{32}. \tag{4.35}$$

Consequently, the CP phase in matter equals

$$\delta^m_D \approx \delta_D - \delta_2$$

in agreement with (4.29) which differs by the small correction due to the matter effect on the 1-3 mixing. Thus, the violation of vacuum mimicking gives the main correction to the CP phase in matter.

2. The interference term is modified by a factor r_V and the solar term by a factor r_V^2. The deviation from the standard case equals

$$r_V^2 - 1 = \xi_{21}|\epsilon'_{12}|(2\cos\phi_\epsilon + \xi_{21}|\epsilon'_{12}|). \tag{4.36}$$

Consequently, the correction vanishes when

$$|\epsilon'_{12}| = -\frac{2\cos\phi_\epsilon}{\xi_{21}}. \tag{4.37}$$

For $\phi_\epsilon = 0$ and π, the factor r_V itself can be zero if

$$|\epsilon'_{12}| = \frac{1}{\xi_{21}} = \frac{\sin 2\theta_{12}}{2x_{21}} = \sin 2\theta_{12}\frac{\Delta m^2_{21}}{4EV}. \tag{4.38}$$

Let us consider the effects of the NSI parameters $\epsilon_{ee} - \epsilon_{\mu\mu}$, $\epsilon_{\tau\tau} - \epsilon_{\mu\mu}$, $\epsilon_{e\mu}$, $\epsilon_{e\tau}$ and $\epsilon_{\mu\tau}$ separately. They modify the $\nu_\mu - \nu_e$ oscillation probability P_μ via ϵ'_{12}, see the second equation of (4.6). Notice that the largest possible NSI parameter $\epsilon_{ee} - \epsilon_{\mu\mu}$ does not contribute to ϵ'_{12}.

From (4.6) we find the parameter of the violation of vacuum mimicking in terms of the NSI parameters:

$$r_V = \left|1 + \frac{2x_{21}F}{\sin 2\theta_{12}}\right|, \quad F = \begin{cases} 0 & \leq \mathcal{O}(\lambda^5) \\[2mm] c_{23}s_{23}s_{13}e^{i\delta_D}(\epsilon_{\tau\tau} - \epsilon_{\mu\mu}) & \leq \mathcal{O}(\lambda^3) \\[2mm] c_{23}c_{13}\epsilon^*_{e\mu} & \leq \mathcal{O}(\lambda) \\[2mm] -s_{23}c_{13}\epsilon^*_{e\tau} & \leq \mathcal{O}(\lambda) \\[2mm] -s_{13}e^{i\delta_D}(\cos 2\theta_{23}\mathbb{R} + i\mathbb{I})(\epsilon_{\mu\tau}) & \leq \mathcal{O}(\lambda^3). \end{cases} \tag{4.39}$$

The presence of several non-zero ϵ can be easily taken into account by summing up the contributions to F.

Let us comment on the effect of individual NSI parameter (4.39) when all others are zero.

- $\epsilon_{ee} - \epsilon_{\mu\mu} \neq 0$. Being the biggest allowed parameter, it generates ϵ'_{11}, ϵ'_{13} and ϵ'_{33} while other ϵ'_{ij} parameters vanish. According to (4.6), the parameter ϵ'_{11} is the diagonal element of the Hamiltonian $\mathcal{H}'_{2\nu}$ while ϵ'_{13} and ϵ'_{33} cannot contribute to $\mathcal{H}'_{2\nu}$. Therefore, vacuum mimicking is realized: $F = 0$ and $r_V = 1$ in the leading order.

- $\epsilon_{\tau\tau} - \epsilon_{\mu\mu} \neq 0$. This parameter contributes to all ϵ'_{ij}. In ϵ'_{12} it appears with suppression factor s_{13}, so that $\epsilon'_{12} = \mathcal{O}(\lambda^3)$. Although $\epsilon_{\tau\tau}$ and $\epsilon_{\mu\mu}$ are the diagonal elements of the matter potential matrix in the flavor basis, they violate vacuum mimicking via ϵ'_{12}. This happens due to the 3ν mixing and large oscillation phase associated with the third state (otherwise mimicking would exist for all mass splittings [49]). We can call such a violation *the induced* violation of vacuum mimicking due to the 3ν mixing. The corresponding contribution to the oscillation probability is proportional to $s_{23}s_{13}$.

- $\epsilon_{e\mu} \neq 0$ produces all ϵ'_{ij} but ϵ'_{22}. It appears in ϵ'_{12} without suppression, and therefore provides the largest violation of vacuum mimicking. Similar statement applies for $\epsilon_{e\tau} \neq 0$.

- $\epsilon_{\mu\tau} \neq 0$ generates all ϵ'_{ij}. Being small it appears with s_{13} in ϵ'_{12}.

In Fig. 3 we show the dependence of $r_V - 1$ on the NSI parameters. According to Fig. 3, in the 1σ allowed interval of $\epsilon_{e\mu}$, the correction is between $\pm 45\%$ at T2K, with maxima at $\mathrm{Arg}[\epsilon_{e\mu}] = 0$ and minimum at $\mathrm{Arg}(\epsilon_{e\mu}) = \pi$. At μDAR, the correction is 12 times smaller: $\pm 4\%$. For $\epsilon_{e\tau}$ the correction at T2K is slightly larger: $\pm 65\%$ with maximum at $\mathrm{Arg}[\epsilon_{e\tau}] = \pi$.

The correction from $\epsilon_{\mu\tau}$ depends on the phase δ_D. For $\delta_D = 3\pi/2$ we have from (4.39)

$$\xi_{21}\epsilon'_{12} = -\xi_{21}s_{13}|\epsilon_{\mu\tau}|(-i\cos 2\theta_{23}\cos\phi_{\mu\tau} + \sin\phi_{\mu\tau}) \approx \xi_{21}s_{13}|\epsilon_{\mu\tau}|\sin\phi_{\mu\tau}$$

which gives a correction between $\pm 1.2\%$. The parameter $(\epsilon_{\tau\tau} - \epsilon_{\mu\mu})$ is real but its correction depends on δ_D. For $\delta_D = 3\pi/2$, we have $r_V = |1 - is_{13}s_{23}c_{23}(\epsilon_{\tau\tau} - \epsilon_{\mu\mu})|$ and consequently $r_V - 1 \approx [s_{13}s_{23}c_{23}(\epsilon_{\tau\tau} - \epsilon_{\mu\mu})]^2$ which is negligible being quadratic in s_{13}.

The Fig. 4 shows the dependence of the correction to the CP phase $\delta_2 \approx \delta_D^m - \delta_D$ on the NSI parameters. The largest correction comes from $\epsilon_{e\mu}$ and $\epsilon_{e\tau}$. With the 1σ interval of $\epsilon_{e\mu}$ we obtain $\delta_2 \approx \pm 30°$ at T2K and $\delta_2 = \pm 2.2°$ at μDAR. Similar numbers are obtained for $\epsilon_{e\tau}$: $\delta_2 \sim \pm 40°$ and
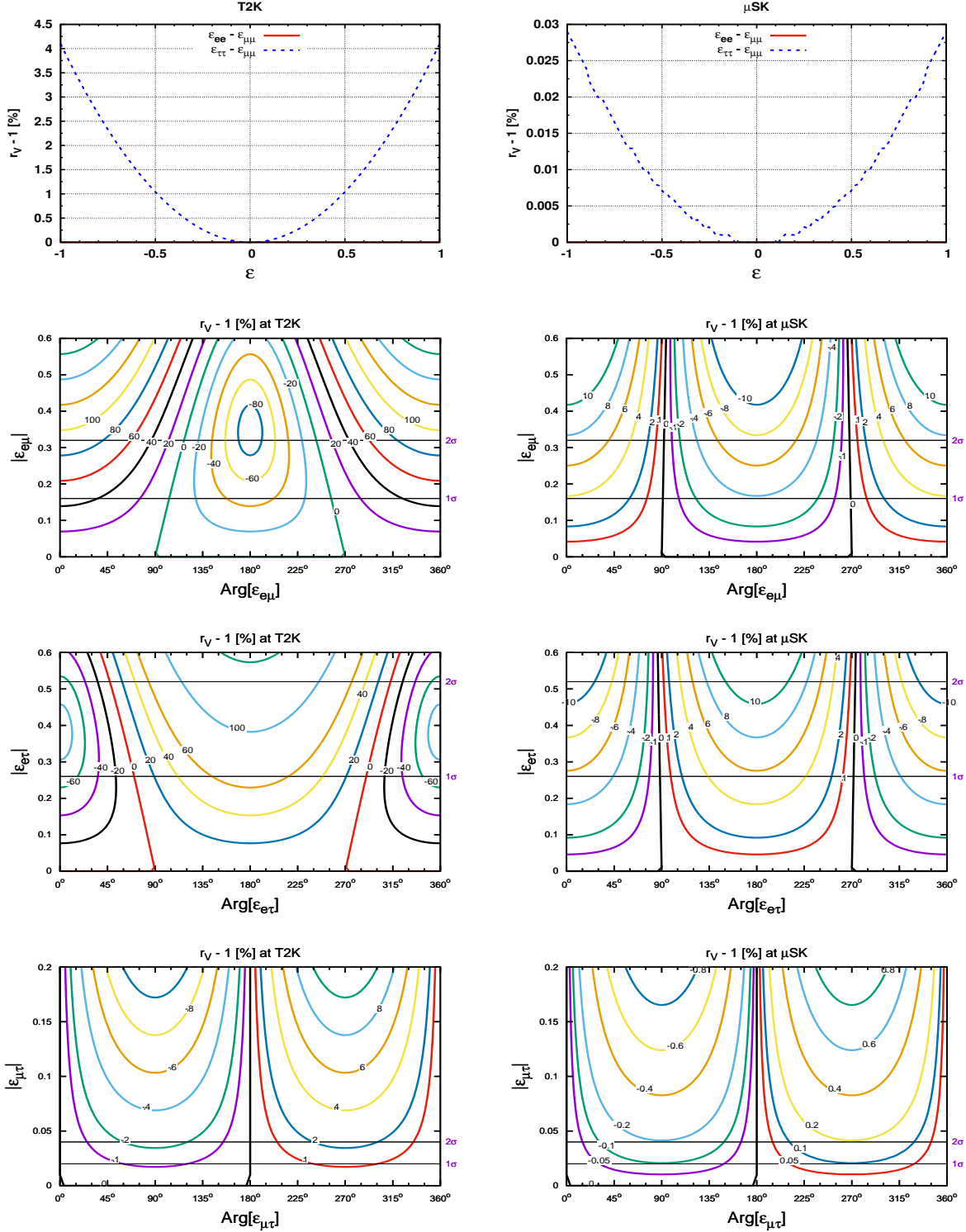
Fig. 3: Dependence of the deviation from vacuum mimicking, $r_V - 1$, on the absolute values and phases of the NSI parameters: (a) $\epsilon_{ee} - \epsilon_{\mu\mu}$ and $\epsilon_{\tau\tau} - \epsilon_{\mu\mu}$; (b) $\epsilon_{e\mu}$; (c) $\epsilon_{e\tau}$; (d) $\epsilon_{\mu\tau}$. We use $\delta_D = 3\pi/2$. The left panels are for $E_\nu = 600\,\text{MeV}$ (T2(H)K) and the right panels are for $E_\nu = 50\,\text{MeV}$ (μSK). The horizontal lines show 1σ and 2σ upper bounds on the NSI parameters.

$\delta_2 = \pm 3°$, respectively. Contrary to the situation for r_V, the parameter $\epsilon_{\tau\tau} - \epsilon_{\mu\mu}$ has larger effect on $\delta_D^m - \delta_D$ than $\epsilon_{\mu\tau}$ does.
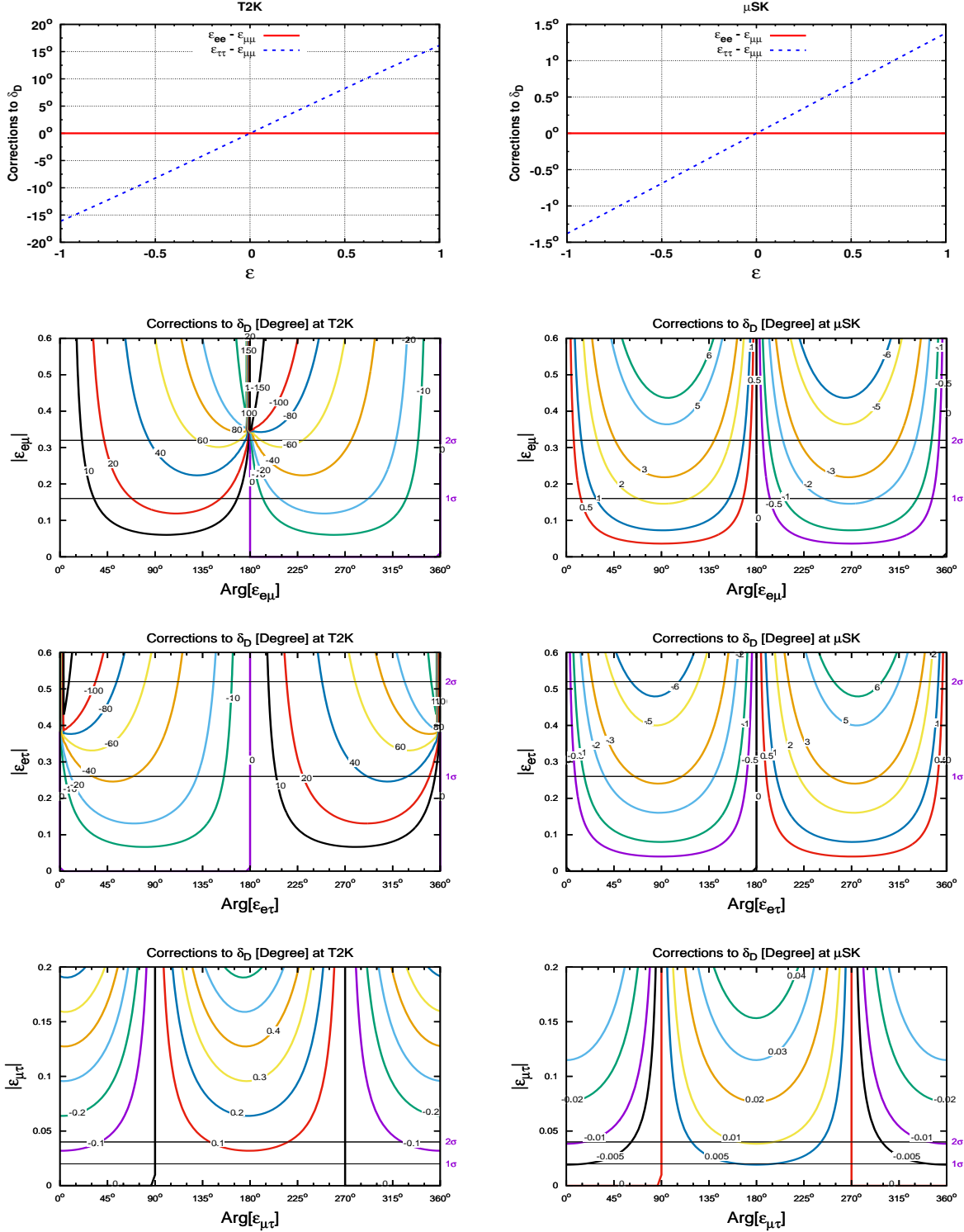
20

Fig. 4: The same as in Fig. 3 for the matter correction to the leptonic Dirac CP phase $\delta_D^m - \delta_D = \delta_2$.

The attraction points in the $\epsilon_{e\mu}$ and $\epsilon_{e\tau}$ planes at $|\epsilon_{e\mu}| \approx -0.35$, $\phi_{e\mu} = \pi$ and $\epsilon_{e\tau} \approx 0.4$, $\phi_{e\tau} = 0, 2\pi$ correspond to $r_V = 0$ for $E_\nu = 600\,\text{MeV}$, according to (4.38). (For μDAR that would appear at much larger, already excluded, values of NSI parameters.) Around the attraction points the correction δ_2 to the CP phase δ_D can take any value.

From the observational point of view the deviation $r_V - 1$ produces an additional degeneracy with δ_D. The factor r_V in the interference term can be absorbed in redefinition of δ_D. Indeed, the interference term is proportional to $r_V \cos(\delta_D - \phi_{32}^m)$ and its variation

$$(r_V - 1)\cos(\delta_D - \phi_{32}^m) - \Delta\delta_D r_V \sin(\delta_D - \phi_{32}^m) \tag{4.40}$$

vanishes when

$$\Delta\delta_D = \cot(\delta_D - \phi_{32}^m)\,\frac{r_V - 1}{r_V}. \tag{4.41}$$

At the first oscillation maximum, $\phi_{32}^m \approx \pi/2$, we obtain

$$\Delta\delta_D = \tan\delta_D\,\frac{r_V - 1}{r_V}. \tag{4.42}$$

Near the maximal CP violation $\delta_D = 3\pi/2$ the correction can be strongly enhanced.

4.3. Corrections to the total oscillation probability

The complete form of the oscillation probability $P_{\mu e}$ is given by the expression (2.33) with oscillation parameters in matter determined in Sec. 4.1. According to (2.33) the following quantities are modified in matter: r_V, $\delta_D^m \approx \delta_D - \delta_2$ which are the parameters of the 1-2 sector, and θ_{13}^m, ϕ_{31}^m, ϕ_{32}^m - the parameters of the 1-3 sector. We will neglect the corrections due to κ as well as due to the matter effect on the 2-3 mixing which is of the order λ^4. In what follows we will consider the NSI corrections due to the modification of these oscillation parameters in order, comparing the oscillation probabilities with ($P_{\mu e}^{NSI}$) and without ($P_{\mu e}$) the NSI effects:

$$\frac{\delta P_{\mu e}}{P_{\mu e}} \equiv \frac{P_{\mu e}^{NSI} - P_{\mu e}}{P_{\mu e}}. \tag{4.43}$$

1. The violation of vacuum mimicking gives two contributions: from $r_V - 1$ and δ_2, both determined by $\epsilon'_{12} \sim \lambda$. They affect the interference term $P_{\mu e}^I$. The violation parameter r_V also modifies the "solar" probability $P_{\mu e}^S$. However, since $P_{\mu e}^S$ itself is very small, the correction to the total probability via $P_{\mu e}^S$ can be neglected.

The correction due to $r_V - 1$ is given by

$$\frac{\delta P_{\mu e}^I}{P_{\mu e}^I} = r_V - 1. \tag{4.44}$$

Since $P_{\mu e}^I \approx (0.25 - 0.30)P_{\mu e}$, the correction can be estimated as $(0.25 - 0.30)(r_V - 1)$. According to the computations in Sec. 4.2, this can lead up to $(10 - 15)\%$ correction for $\epsilon_{e\mu}$ and $(15 - 22)\%$ for $\epsilon_{e\tau}$ at T2K in the 1σ allowed intervals. In comparison, the corrections are about 12 times smaller at μSK. They strongly depend on the phases of $\epsilon_{\alpha\beta}$ and the phase δ_D.

The correction due to δ_2 is given by

$$\frac{\delta P_{\mu e}^I}{P_{\mu e}^I} = \tan(\delta_D - \delta_2 - \phi_{32}^m)\,\delta_2 \tag{4.45}$$

with δ_2 defined in (4.14) being roughly proportional $\mathbb{I}(\epsilon_{12}')$. Then the correction to the total probability is suppressed by a factor of $\tan(\delta_D - \delta_2 - \phi_{32}^m) \approx 1/4 \sim 1/3$. As a result, the contribution from δ_2 is somewhat smaller than that from $(r_V - 1)$, reaching $(5 - 10)\%$ at T2K.

2. The correction due to the NSI matter effect on the 1-3 mixing. Using Eqs. (4.30) and (4.10), we can write the correction to the mixing angle in matter $\theta_{13}^{m,SI}$ with standard interaction as

$$\delta\theta_{13}^m = \theta_{13}^m - \theta_{13}^{m,SI} = x_{31}\left[\cos\delta_3 |s_{13}c_{13} + \epsilon_{13}'| - s_{13}c_{13}\right]. \tag{4.46}$$

Thus, $\delta\theta_{13}^m$ depends on $(\epsilon_{12}', \epsilon_{13}') \sim \lambda$ (i.e., on different combination of the NSI parameters). According to (4.46), $\delta\theta_{13}^m \sim B s_{13} r_\Delta$ with $B \sim 4 - 6$ at T2K and $B \approx 1$ at μSK.

The corrections to the 1-3 mixing can contribute to the "atmospheric" probability as

$$\frac{\delta P_{\mu e}^A}{P_{\mu e}^A} \approx 4\cot 2\theta_{13}\delta\theta_{13}^m \sim B r_\Delta. \tag{4.47}$$

For the interference term the relative correction is 2 times smaller and the contribution to the total probability is further suppressed by a factor $1/4 \sim 1/3$. The total correction to $P_{\mu e}$ due to $\delta\theta_{13}^m$ can be as large as $(10 \sim 15)\%$.

3. The correction via the 1-3 oscillation phase. The modification of the 3-1 phase due to NSI is

$$\delta\phi_{13}^m = \phi_{13}^{m,NSI} - \phi_{13}^m = (\Delta H_{31}^{NSI} - \Delta H_{31})\frac{L}{2}. \tag{4.48}$$

Using (4.15) we obtain

$$\Delta H_{31} - \Delta H_{31}^0 = \frac{1}{2}V(2\epsilon_{33}' - \epsilon_{11}' - \epsilon_{22}') + \frac{1}{2}[\Delta H_{21} - \Delta H_{21}^0], \tag{4.49}$$

where ΔH_{21} is defined in (4.14), ΔH_{31}^0, ΔH_{21}^0 are splittings between the eigenvalues without NSI ($\epsilon = 0$). In turn, being in general of the order $V\epsilon$, see (4.14), $\Delta H_{21} - \Delta H_{21}^0 \approx -V\cos 2\theta_{12}\epsilon_{11}'$ below the 1-2 resonance and $\Delta H_{21} - \Delta H_{21}^0 \to V\epsilon_{11}'$ above the resonance. In the second case there is a cancellation between the last term in (4.49) with $V\epsilon_{11}'$ in the first term there. Thus, the phase difference becomes

$$\delta\phi_{13}^m \approx h\frac{VL}{4} \sim r_\Delta, \tag{4.50}$$

where the coefficient h is smaller than 1 and can be suppressed at high energies. Notice that $\delta\phi_{13}^m$ depends not only on $\epsilon_{11}' = O(1)$ but also on other diagonal elements ϵ_{22}', $\epsilon_{11}' \sim \lambda^2$. So, $\delta\phi_{13}^m \sim r_\Delta$.
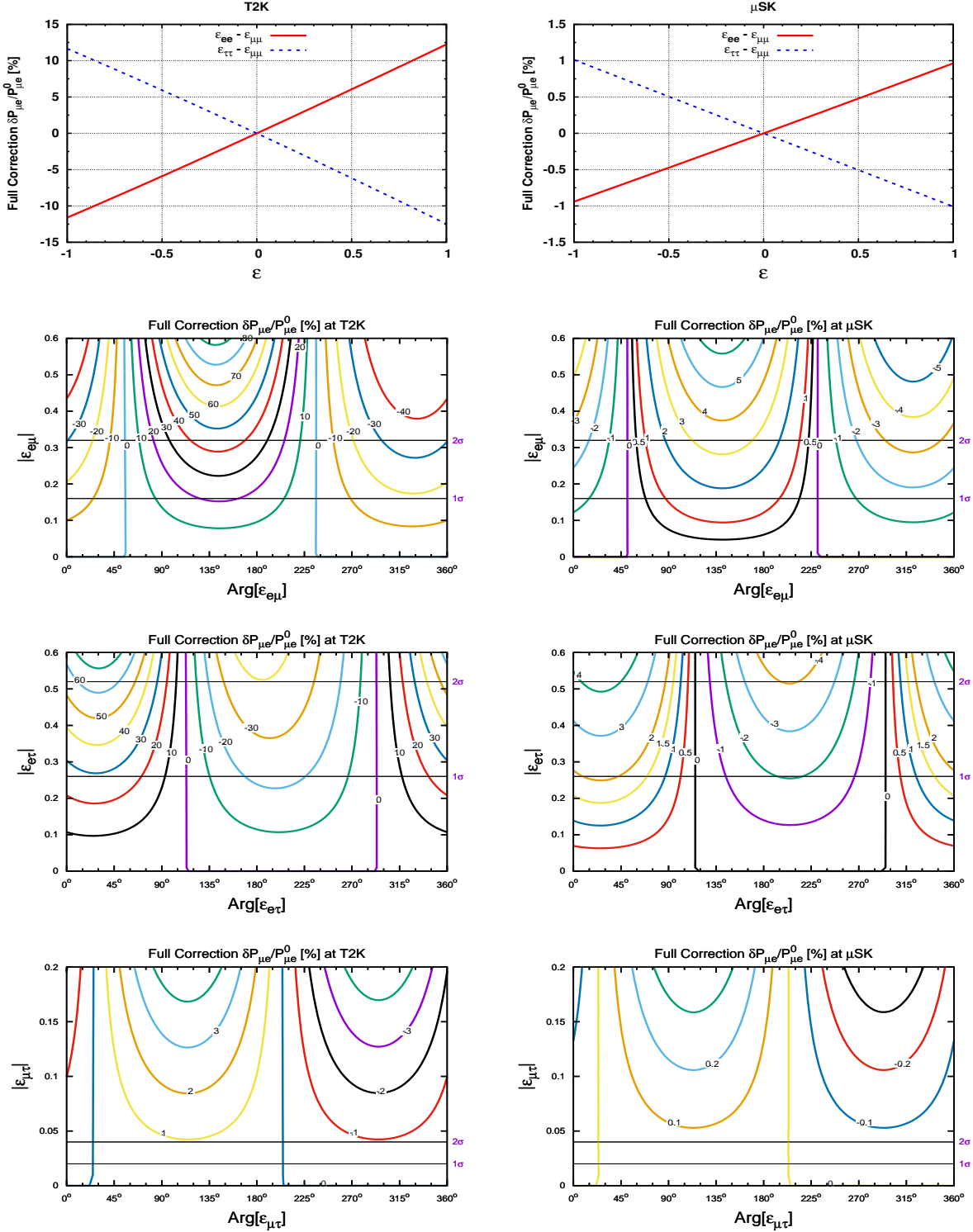
Fig. 5: The dependence of the corrections to total oscillation probability $P_{\mu e}$ on values of NSI parameters: (a) $\epsilon_{ee} - \epsilon_{\mu\mu}$ and $\epsilon_{\tau\tau} - \epsilon_{\mu\mu}$; (b) $\epsilon_{e\mu}$; (c) $\epsilon_{e\tau}$; (d) $\epsilon_{\mu\tau}$ with $\delta_D = -90°$ and $\rho_m = 3\text{g/cm}^3$. The left panels are for $E_\nu = 600\,\text{MeV}$ and $L = 295\,\text{km}$ at T2(H)K while the right panels are for $E_\nu = 50\,\text{MeV}$ and $L = 23\,\text{km}$ at μSK.

The correction to the "atmospheric" probability equals

$$\frac{\delta P^A_{\mu e}}{P^A_{\mu e}} \approx 2\cot\phi_{13}\ \delta\phi^m_{13}. \tag{4.51}$$

At the first oscillation maximum an additional suppression comes from $\cot\phi_{13} \approx 0$.

The analytic consideration presented here allows us to reproduce the results of numerical computations and analyse their dependence on the NSI parameters. In general, the violation of vacuum mimicking gives substantial or even dominant contribution to the probability change. The largest corrections come from $r_V - 1$, δ_2, and $\delta\theta_{13}^m$. Their relative contributions depend on the phases of ϵ's. For $\text{Arg}[\epsilon_{e\mu}] \sim 0$ or π the violation of vacuum mimicking gives the main contribution, which is however suppressed at $\text{Arg}[\epsilon_{e\mu}] \sim \pi/2$, $3\pi/2$. If the NSI parameters are such that $\epsilon'_{12} = 0$, the main contribution to $P_{\mu e}$ comes from the 1-3 mixing determined by ϵ'_{13}. And *vice versa* if $\epsilon'_{13} = 0$, the effect of 1-3 mixing is suppressed and contributions from $r_V - 1$ and δ_2 dominate, *etc.*

These features are in agreement with our numerical computations. With all the contributions combined, the total effect of NSI parameters is shown in Fig. 5. Although the NSI parameter $\epsilon_{ee} - \epsilon_{\mu\mu}$ does not contribute to the deviation from vacuum mimicking (see Fig. 3) or to the leptonic Dirac CP phase (see Fig. 4), it affects the total oscillation probability $P_{\mu e}$, mainly due to the correction $\delta\theta_{13}^m$ in (4.47), which is suppressed by s_{13}. The main contribution to the corrections comes from $\epsilon_{e\mu}$ and $\epsilon_{e\tau}$, reaching 20% and 30%, respectively, for the 1σ upper bounds. The contribution from $(\epsilon_{ee} - \epsilon_{\mu\mu}, \epsilon_{\tau\tau} - \epsilon_{\mu\mu}, \epsilon_{\mu\tau})$ can be as large as $(5 - 10)\%$.

5. CP Measurement in the Presence of Non-Standard Interactions

In this section we use T2K and μSK as examples to illustrate the NSI effect on the measurement of the genuine Dirac CP phase δ_D. To estimate the CP sensitivity we have simulated the pseudo-data at T2K and μDAR for presently favored "true" value $\delta_D = 3\pi/2$. We take the following values of the neutrino oscillation parameters

$$\sin^2 2\theta_{13} = 0.089 \pm 0.005\,, \quad \sin^2 2\theta_{12} = 0.857 \pm 0.024\,, \quad \sin^2 2\theta_{23} = 0.5 \pm 0.055\,, \tag{5.1a}$$

$$\Delta m_{21}^2 = (7.5 \pm 0.2) \times 10^{-5}\text{eV}^2\,, \quad \Delta m_{31}^2 = (2.4 \pm 0.1) \times 10^{-3}\text{eV}^2\,, \tag{5.1b}$$

to be consistent with the setup in [44]. The pseudo-data is simulated in the absence of NSI.

We use the following χ^2 function

$$\chi^2 \equiv \chi_{stat}^2 + \chi_{sys}^2 + \chi_{prior}^2 \tag{5.2}$$

to fit the pseudo-data, with or without NSI. Here χ_{stat}^2 corresponds to statistical errors: $\chi_{stat}^2 \equiv \sum_i (N_i^{data} - N_i^{fit})^2 / N_i^{data}$ while $\chi_{sys}^2 = \sum_i [(f_i - 1)/\delta f]^2$ accounts for the systematical uncertainty in the neutrino fluxes from the J-PARC and μDAR neutrino sources. The J-PARC flux has 5%

uncertainty for both neutrino and anti-neutrino modes, also for the μDAR flux we take about 5% [2] uncertainty, see [44] for details. Finally, the prior part χ^2_{prior} takes into account our current knowledge of the neutrino oscillation parameters in vacuum (5.1) and the prior constraints (4.2) on the NSI parameters. The later is included only when we fit the pseudo-data with the NSI parameters.

In simulations we used both the neutrino and antineutrino channels. Recall that the standard oscillation probability (2.33) at the first oscillation maximum corresponding to $\phi^m_{31} = \pi/2$ and $\phi^m_{21} \approx r_\Delta \times \pi/2$ can be approximated as

$$P_{\mu e} \approx s^2_{23} \sin^2 2\theta^m_{13} \pm c^m_{13} \sin 2\theta^m_{13} \sin 2\theta_{23} \sin 2\theta_{12} \frac{\pi}{2} r_\Delta \sin \delta_D \,, \tag{5.3}$$

where $\pm$ stand for neutrinos and anti-neutrinos, respectively. The first term in (5.3) is larger than the second term by a factor of $s_{13}/r_\Delta \sim 5$. This magnifies the effect of the uncertainties in the first term. The largest one appears in the 2-3 mixing, s_{23}. Around the maximal mixing, $\sin 2\theta_{23} \approx 1$, the variations of s^2_{23} are enhanced with respect to the variations of $\sin 2\theta_{23}$: $\Delta(s^2_{23}) \approx \Delta(\sin 2\theta_{23}) \times (\sin 2\theta_{23}/2 \cos 2\theta_{23}) \gg \Delta(\sin 2\theta_{23})$. Consequently, a small uncertainty in $\sin 2\theta_{23}$ propagates to a large uncertainty in s_{23}. It effectively reduces the sensitivity to δ_D which originates from the second term in (5.3). Running T2K in both neutrino and anti-neutrino modes can avoid this problem. With both $P_{\mu e}$ and $P_{\bar\mu\bar e}$ measured, the difference between them is purely the CP violating term that is proportional to $\sin \delta_D$.

The results in this section are simulated by the NuPro package [65].

5.1. The CP sensitivity at T2K in the presence of NSI

In simulations for T2K we use 7.8×10^{21} proton on target (POT) for the J-PARC flux, corresponding to 342 events in the neutrino mode or 83 events in the anti-neutrino mode for $\delta_D = 3\pi/2$ [66]. As discussed above, to reduce uncertainties in the determination of δ_D at T2K, it is necessary to run the experiment in both neutrino and anti-neutrino modes. However, in both production and detection, the cross sections for anti-neutrinos are smaller than those for neutrinos. To collect comparable number of events, and hence balance the statistical uncertainty in both modes, the antineutrino mode should run longer. Therefore, in simulations we use 2 years of running in the neutrino mode and 4 years in the antineutrino mode. Correspondingly, 114 neutrino events and 56 antineutrino events are expected.

We compute the minimal χ^2 value as a function of the fit value of the phase δ^{fit}_D, with and without

---

[2]If the near detector μNear [64] is also implemented, the μDAR flux uncertainty can be significantly reduced.
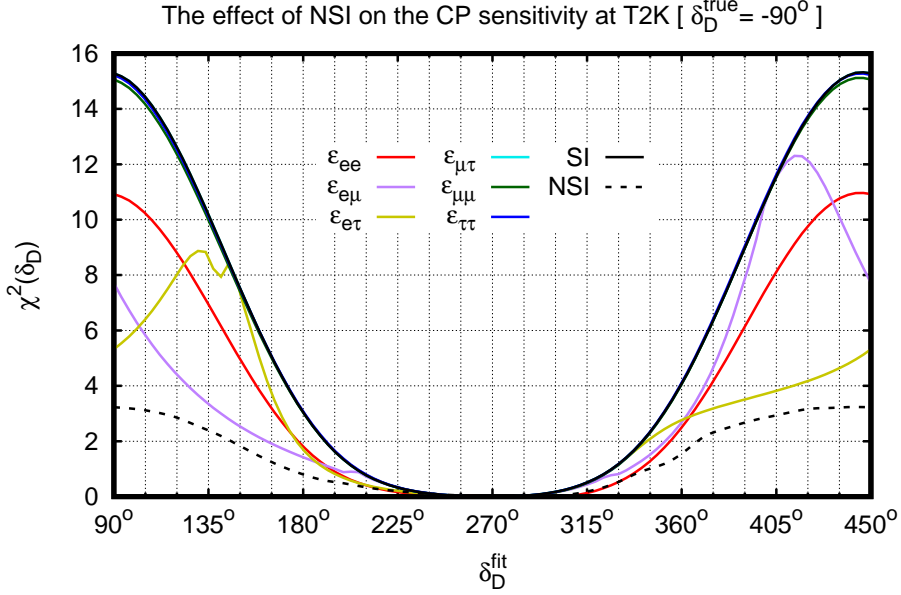
Fig. 6: The effect of NSI on the CP sensitivity at T2K with 2 years of running for the neutrino mode and 4 years for the antineutrino mode, with the prior constraints (4.2). The pseudo-data with standard interaction and $\delta_D^{true} = 3\pi/2$ is fit with standard interaction (SI) as well as with individual NSI parameters (ϵ_{ee}, $\epsilon_{e\mu}$, $\epsilon_{e\tau}$, $\epsilon_{\mu\tau}$, $\epsilon_{\mu\mu}$, $\epsilon_{\tau\tau}$) and full set of NSI parameters (dashed line).

the NSI parameters. The results are shown in Fig. 6. The solid black line in Fig. 6 presents the CP sensitivity at T2K without NSI. We can see that this line is nearly symmetric with respect to $\delta_D^{fit} = \delta_D^{true} = 3\pi/2$ which is related to the degeneracy between δ_D and $\pi - \delta_D$ due to the $\sin \delta_D$ dependence in the oscillation probability (5.3). According to Fig. 6, the true value $\delta_D^{true} = 3\pi/2$ can be distinguished from $\delta_D^{fit} = 0$ (π) by $\chi^2 = 3$ (1.7σ) and from $\delta_D^{fit} = \pi/2$ by $\chi^2 = 15$ (3.8σ). The results can be easily scaled for higher statistics at T2HK or T2K-II.

The sensitivity to δ_D can be significantly undermined by NSI. In Fig. 6 we show the dependence of χ^2 on the fit value δ_D^{fit} for different NSI parameters separately, although only two combinations of the three diagonal elements (ϵ_{ee}, $\epsilon_{\mu\mu}$, and $\epsilon_{\tau\tau}$) affect oscillations, as we used in Sec. 2. The color curves in Fig. 6 show that the CP sensitivity at T2K is significantly reduced by ϵ_{ee}, $\epsilon_{e\mu}$, and $\epsilon_{e\tau}$, but almost not affected by $\epsilon_{\mu\mu}$, $\epsilon_{\mu\tau}$, $\epsilon_{\tau\tau}$. This is because $\epsilon_{\tau\tau} - \epsilon_{\mu\mu}$ and $\epsilon_{\mu\tau}$ are constrained much stronger according to (4.2) and also their contributions to ϵ'_{12} are suppressed by s_{13}, see (4.6). Consequently, they have small contribution to the violation of vacuum mimicking via r_V (4.32) and to the Dirac CP phase via δ_2 (4.14). Although $\epsilon_{ee} - \epsilon_{\mu\mu}$ cannot contribute to the leading order corrections via the Dirac CP phase δ_D^m and r_V, see (4.39), its effect on the oscillation probability via $\delta\theta_{13}^m$ (4.46) as a function of ϵ'_{13} (4.6) can still be significant due to weak prior constraint (4.2). For $\epsilon_{e\mu}$ and $\epsilon_{e\tau}$, the prior constraints are stronger but their contributions are not suppressed in ϵ'_{12}, see (4.6).

The non-vanishing ϵ_{ee}, $\epsilon_{e\mu}$, $\epsilon_{e\tau}$ reduce the distinguishability between $\delta_D^{fit} = 0$ (π) and $\delta_D^{true} = 3\pi/2$ from $\chi^2 = 3$ to 1.7 (1.3σ). The difference between the two maximal CP values $\delta_D = \pm\pi/2$ decreases from $\chi^2 \approx 15$ (roughly 4σ) to $\chi^2 \approx 5.5$ (2.3σ). If all NSI parameters are present, the CP sensitivity at T2K can be further reduced as is shown by the dashed black line in Fig. 6. The distinguishability of $\delta_D^{fit} = \pi/2$ from $\delta_D^{true} = 3\pi/2$ is reduced by roughly a factor of 5 to $\chi^2 \approx 3.2$ (1.8σ) and for $\delta_D^{fit} = 0$ (π) it becomes $\chi^2 \approx 0.8$ (0.9σ). The value of χ^2 for $\delta_D^{fit} = 0$ (π) and the corresponding best-fit values of the NSI parameters are shown in Table 1.

5.2. Improving the CP sensitivity with neutrinos from μDAR

Due to smaller energies, $\sim 50\,\mathrm{MeV}$, as compared with the peak energies, $\sim 600\,\mathrm{MeV}$, of the J-PARC flux, neutrinos of the μDAR flux will experience 12 times smaller matter effect than in T2(H)K. In simulation we use the characteristics proposed for μSK [44] which includes the existing Super-K detector and a $9\,\mathrm{mA}$ cyclotron to produce $\bar\nu_\mu$ from μDAR. The optimal distance between the μDAR source and the SK detector is around $23\,\mathrm{km}$. For 6 years of running, a total number 1.1×10^{25} POT can be collected, corresponding to 212 $\bar\nu_\mu \to \bar\nu_e$ oscillation events in the SK detector for $\delta_D^{true} = 3\pi/2$.
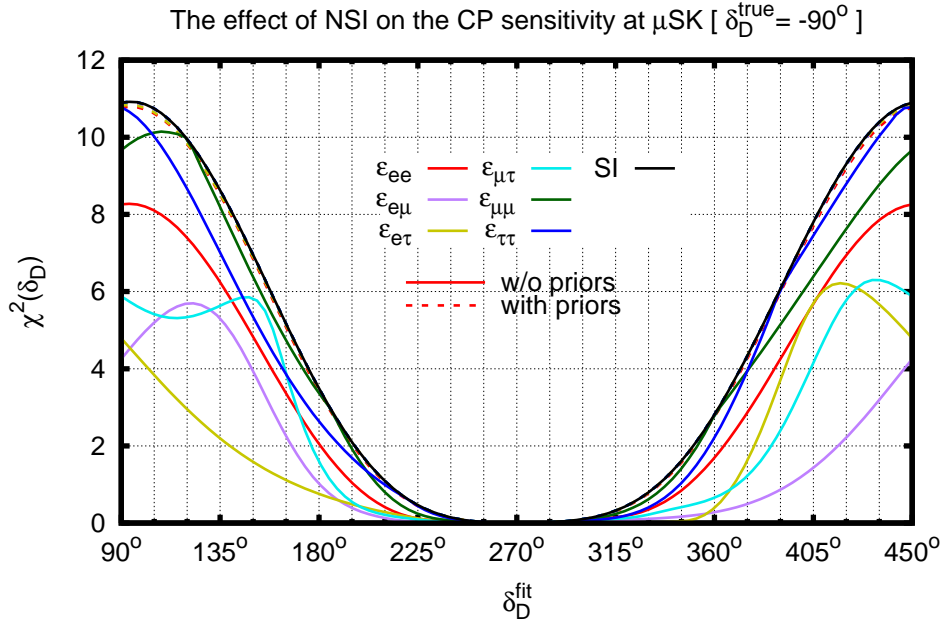

Fig. 7: The effect of NSI on the CP sensitivity at μSK with 6 years of running in the antineutrino mode, without (solid lines) and with (dashed line) the prior constraints (4.2).

In Fig. 7, we show the CP sensitivity at μSK. Without NSI the true value $\delta_D^{true} = 3\pi/2$ can be distinguished from $\delta_D^{fit} = 0$ or π by $\chi^2 = 2.8$ (1.7σ) and from $\delta_D^{fit} = \pi/2$ by $\chi^2 = 11$ (3.3σ). Notice that the curve is not symmetric with respect to $\delta_D = 3\pi/2$ due to the interplay between the $\sin\delta_D$

and $\cos \delta_D$ dependences in the oscillation probability $P_{\bar{\mu}\bar{e}}$.

The matter effects at μSK are an order of magnitude smaller than at T2K, and consequently the sensitivity to δ_D is less affected by NSI, in comparison with Fig. 6. With the prior constraint (4.2) imposed, the sensitivity to δ_D at μSK is almost unaffected. The sensitivity to δ_D is significantly reduced by the NSI parameters only if no prior constraint is imposed. Even in this case the sensitivity to δ_D is not reduced to almost zero by the NSI parameters (ϵ_{ee}, $\epsilon_{e\mu}$, $\epsilon_{e\tau}$), which is the case at T2K.

Let us consider the sensitivity to δ_D of the combined measurements at TNT2K [44]. While T2K unavoidably measures both δ_D and NSI, μSK mainly provides a determination of the phase δ_D. The Fig. 8 shows how μSK can improve the sensitivity to δ_D, in comparison with Fig. 6 from T2K only. With the prior constraints (4.2) imposed, the significance of distinguishing $\delta_D^{true} = 3\pi/2$ from $\delta_D^{fit} = \pi/2$ can reach 5σ and the distinguishability from vanishing CP values, $\delta_D = 0$ or π, can be about 2.5σ for individual NSI parameters. The numbers become 4.6σ and 2.2σ with the full set of NSI parameters, in comparison with 1.8σ and 0.9σ at T2K as well as 3.3σ and 1.7σ at μSK. Combining the T2K and μSK results will substantially improve the sensitivity to δ_D, in comparison to the sensitivity of T2K or μSK alone.

With a μDAR antineutrino source built near the Super-K/Hyper-K detectors, T2(H)K can devote all its exposure time to the neutrino run. This can significantly increase the event number. We can obtain a factor of 3 increase in the number of neutrino events and a factor of 4 increase in the number of antineutrino events in comparison to those at T2K. In addition, the wide energy spectrum of the μDAR antineutrino will break the degeneracy between δ_D and $\pi - \delta_D$ by providing $\cos \delta_D$ dependence of $P_{\mu e}$, especially for non-maximal CP phase, $\delta_D \neq \pi - \delta_D$. If the CP phase happens to be $\delta_D = \pm\pi/2$, μSK can also reduce the uncertainty around $\delta_D^{true} = 3\pi/2$ [44]. With mainly $\sin \delta_D$ dependence at T2K, the CP uncertainty $\Delta(\delta_D) \propto 1/\cos \delta_D$ diverges for maximal CP violation. This can be significantly improved due to the $\cos \delta_D$ dependence provided by the μDAR flux.

In the right panel of Fig. 8 we show the CP sensitivity of the combined measurement with T2K running 6 years purely in the neutrino mode (νT2K) and μSK running 6 year purely in the antineutrino mode. The latter CP sensitivity is higher than the sensitivity of the combination of T2K (neutrino and antineutrino) and μSK. Without NSI, the distinguishability of $\delta_D^{fit} = \pi/2$ from $\delta_D^{true} = 3\pi/2$ increases from around 6σ to around 8σ. After including individual NSI parameter, it increases from 5σ to 5.4σ with prior constraints. The distinguishability of $\delta_D^{fit} = 0$ or π from $\delta_D^{true} = 3\pi/2$ increases from 3.3σ to 4σ for SI and from 2.6σ to 2.8σ for individual NSI parameter with prior constraints. Thus the combination of νT2K (fully neutrino running) and μSK, is better
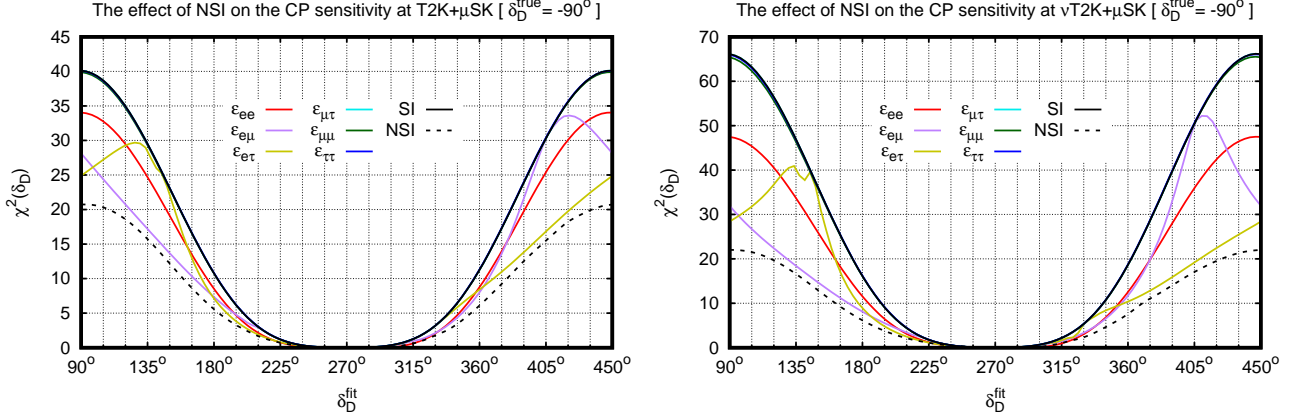
Fig. 8: The effect of NSI on the CP sensitivity at TNT2K with the prior constraints (4.2). For comparison, the same configuration of T2K as in Fig.6, 2 years of running in the neutrino mode and 4 years for anti-neutrino, has adopted in the left panel (T2K) while the right takes 6 years of running in the neutrino mode (νT2K). For both panels, the μSK experiment runs for 6 years in the anti-neutrino mode. The pseudo-data with standard interaction and $\delta_D^{true} = -90°$ is fit with standard interaction (SI), individual NSI parameters (ϵ_{ee}, $\epsilon_{e\mu}$, $\epsilon_{e\tau}$, $\epsilon_{\mu\tau}$, $\epsilon_{\mu\mu}$, $\epsilon_{\tau\tau}$), or full set of NSI parameters (dashed line).

than splitting the T2K run among neutrino and antineutrino modes. Comparing the solid black curve for SI and the dashed one for the full set of NSI parameters, we find that the distinguishability of $\delta_D^{fit} = \pi/2$ from $\delta_D^{true} = 3\pi/2$ decreases from $\chi^2 \approx 40$ to 21 at T2K (2 + 4 years) + μSK, while it decreases from around 65 to 22 for νT2K + μSK. In both cases the CP violation can be established at more than 4.5σ. Although the CP sensitivity with NSI is roughly the same for T2K+μSK and νT2K+μSK, it can be significantly increased at νT2K if there is no NSI.

6. Conclusions

We explored the CP violation and the matter effects in neutrino oscillation in the presence of standard and non-standard interactions at low energies and relatively small baselines. This experimental setup is realized in T2K, the experiments based on μDAR, *etc.* A simple analytic formalism is elaborated which describes the NSI effects and their dependence on the parameters of NSI interactions. The vacuum mimicking and its violation in the 1-2 sector as well as the use of the separation basis play central roles in the formalism.

In the case of standard interactions due to vacuum mimicking the matter affects the oscillation probability $P_{\mu e}$ mainly via the correction to the 1-3 mixing. We find that matter changes the probability by about 13% at T2K and 1% at μDAR. Also we show that vacuum mimicking provides a simple explanation of the fact that the usual formula for $3\nu-$ oscillation probability gives a very

$\delta_D^{true} = -90° $ vs $\delta_D^{fit} = 0°$	T2K		μSK		T2K+μSK		νT2K+μSK	
Event Numbers	$114\nu + 56\bar{\nu}$		$212\bar{\nu}$		$57\nu + 268\bar{\nu}$		$342\nu + 212\bar{\nu}$	
χ^2 for **SI** & **NSI**	4.08	1.54	2.81	2.75	11.3	6.10	18.7	7.59
χ^2	2.50	–	2.75	–	8.77	–	12.5	–
$\epsilon_{ee}^{\rm bf}$	0.69	0.57	0.48	0.47	0.81	0.63	1.07	0.70
χ^2	4.06	–	2.81	–	11.3	–	18.6	–
$\epsilon_{\mu\mu}^{\rm bf}$	-0.02	-0.01	-0.02	-0.01	-0.02	-0.01	-0.02	-0.01
χ^2	4.11	–	2.81	–	11.3	–	18.7	–
$\epsilon_{\tau\tau}^{\rm bf}$	0.02	0.01	0.02	0.01	0.02	0.01	0.01	0.01
χ^2	2.68	–	2.81	–	8.01	–	11.7	–
$\epsilon_{e\mu}^{\rm bf}$	0.12	0.07	0.01	0.01	0.19	0.11	0.23	0.10
χ^2	2.77	–	2.81	–	8.42	–	10.4	–
$\epsilon_{e\tau}^{\rm bf}$	0.25	0.14	0.01	0.01	0.37	0.21	0.51	0.30
χ^2	4.08	–	2.81	–	11.3	–	18.7	–
$\epsilon_{\mu\tau}^{\rm bf}$	0	0	0	0	0	0	0	0

Table 1: The χ^2_{min} and best fit values of the NSI parameters when using $\delta_D^{fit} = 0°$ to fit the pseudo-data generated with SI and $\delta_D^{true} = -90°$, under the prior constraints (4.2). In each experimental configuration T2K, μSK, T2K+μSK, and νT2K+μSK, the χ^2 for **SI** comes from the fit with standard interaction, **NSI** with either individual or the full set of $(\epsilon_{ee}, \epsilon_{e\mu}, \epsilon_{e\tau}, \epsilon_{\mu\tau}, \epsilon_{\mu\mu}, \epsilon_{\tau\tau})$.

good description at energies around the 1-2 resonance.

In the presence of NSI, the vacuum mimicking in the 1-2 sector is strongly broken. The breaking shows up in a very specific way and is related to the single NSI parameter ϵ'_{12} in the separation basis. The same parameter ϵ'_{12} controls the additional contribution to the effective CP phase in matter. The 1-3 mixing is modified by another parameter ϵ'_{13} while the 1-3 oscillation phase is corrected by the diagonal elements ϵ'_{11}, ϵ'_{22} and ϵ'_{33}.

We show that the total probability $P_{\mu e}$ is mainly affected by the violation of vacuum mimicking parametrized by $(r_V - 1)$ and δ_2 as well as by the correction to the 1-3 mixing, $\delta\theta_{13}^m$. The relative effects of the violation of vacuum mimicking and $\delta\theta_{13}^m$ on $P_{\mu e}$ depend on the phases of $\epsilon'_{e\mu}$ or/and $\epsilon'_{e\tau}$. Within the 1σ intervals, the correction to $P_{\mu e}$ due to NSI can reach $(20 - 30)\%$ at T2K and 2% at μDAR. The corrections to the CP phase can be as large as $(40 - 50)°$ at T2K and $3°$ at μDAR.

We apply our analytic formalism to the CP phase measurement at low energies. The standard interaction leads to vacuum mimicking in the solar amplitude and keeps the Dirac CP phase δ_D unaffected. On the contrary, NSI can introduce significant deviation from vacuum mimicking, and consequently, modify δ_D to practically any value at T2K. With prior constraints (4.2) on the size of

NSI parameters, the CP sensitivity in terms of $\chi^2(\delta_D)$ at T2K can be reduced by almost a factor of 2∼3. The effect of NSI can be even larger at NOνA and DUNE with higher neutrino energies.

We show that TNT2K – the combination of T2K and the new component μSK can resolve the δ_D–NSI degeneracy. The μSK component uses the SK detector to study the oscillations of the antineutrinos from a μDAR source. Since the μDAR flux has 10 times lower energy, the effect of NSI at μSK is much smaller than at T2K. While T2K measures both the genuine CP phase δ_D and NSI, μSK can provide clean determination of δ_D simultaneously. The sensitivity to δ_D which can be achieved by this combination of T2K and μSK is much higher than the sensitivity of T2K or μSK alone. The TNT2K configuration can guarantee high sensitivity to δ_D in the presence of NSI.

7. Acknowledgements

References

[1] L. Wolfenstein. Neutrino Oscillations in Matter. *Phys. Rev.*, D17:2369–2374, 1978.

[2] M. M. Guzzo, A. Masiero, and S. T. Petcov. On the MSW effect with massless neutrinos and no mixing in the vacuum. *Phys. Lett.*, B260:154–160, 1991.

[3] Esteban Roulet. MSW effect with flavor changing neutrino interactions. *Phys. Rev.*, D44:R935–R938, 1991.

[4] Tommy Ohlsson. Status of non-standard neutrino interactions. *Rept. Prog. Phys.*, 76:044201, 2013.

[5] O. G. Miranda and H. Nunokawa. Non-standard neutrino interactions: current status and future prospects. *New J. Phys.*, 17(9):095002, 2015.

[6] M. C. Gonzalez-Garcia, Y. Grossman, A. Gusso, and Y. Nir. New CP violation in neutrino oscillations. *Phys. Rev.*, D64:096006, 2001.

[7] A. M. Gago, H. Minakata, H. Nunokawa, S. Uchinami, and R. Zukanovich Funchal. Resolving CP Violation by Standard and Nonstandard Interactions and Parameter Degeneracy in Neutrino Oscillations. *JHEP*, 01:049, 2010.

[8] P. Coloma, A. Donini, J. Lopez-Pavon, and H. Minakata. Non-Standard Interactions at a Neutrino Factory: Correlations and CP violation. *JHEP*, 08:036, 2011.

[9] Y. Itow et al. The JHF-Kamioka neutrino project. In *Neutrino oscillations and their origin. Proceedings, 3rd International Workshop, NOON 2001, Kashiwa, Tokyo, Japan, December 508, 2001*, pages 239–248, 2001.

[10] D. S. Ayres et al. NOvA: Proposal to build a 30 kiloton off-axis detector to study $\nu_\mu \to \nu_e$ oscillations in the NuMI beamline. 2004.

[11] Ko Abe et al. Sensitivity of the T2K accelerator-based neutrino experiment with an Extended run to 20×10^{21} POT. 2016.

[12] Ko Abe et al. Proposal for an Extended Run of T2K to 20×10^{21} POT. 2016.

[13] K. Abe et al. Letter of Intent: The Hyper-Kamiokande Experiment — Detector Design and Physics Potential. 2011.

[14] Kaoru Hagiwara. Physics prospects of future neutrino oscillation experiments in Asia. *Nucl. Phys. Proc. Suppl.*, 137:84–103, 2004.

[15] Masaki Ishitsuka, Takaaki Kajita, Hisakazu Minakata, and Hiroshi Nunokawa. Resolving neutrino mass hierarchy and CP degeneracy by two identical detectors with different baselines. *Phys. Rev.*, D72:033003, 2005.

[16] Kaoru Hagiwara, Naotoshi Okamura, and Ken-ichi Senda. Solving the neutrino parameter degeneracy by measuring the T2K off-axis beam in Korea. *Phys. Lett.*, B637:266–273, 2006. [Erratum: Phys. Lett.B641,491(2006)].

[17] Kaoru Hagiwara, Naotoshi Okamura, and Ken-ichi Senda. Physics potential of T2KK: An Extension of the T2K neutrino oscillation experiment with a far detector in Korea. *Phys. Rev.*, D76:093002, 2007.

[18] Takaaki Kajita, Hisakazu Minakata, Shoei Nakayama, and Hiroshi Nunokawa. Resolving eightfold neutrino parameter degeneracy by two identical detectors with different baselines. *Phys. Rev.*, D75:013006, 2007.

[19] Kaoru Hagiwara and Naotoshi Okamura. Re-evaluation of the T2KK physics potential with simulations including backgrounds. *JHEP*, 07:031, 2009.

[20] Kaoru Hagiwara, Takayuki Kiwanami, Naotoshi Okamura, and Ken-ichi Senda. Physics potential of neutrino oscillation experiment with a far detector in Oki Island along the T2K baseline. *JHEP*, 06:036, 2013.

[21] Kaoru Hagiwara, Pyungwon Ko, Naotoshi Okamura, and Yoshitaro Takaesu. Revisiting T2KK and T2KO physics potential and ν_μ - $\bar\nu_\mu$ beam ratio. 2016.

[22] C. Adams et al. The Long-Baseline Neutrino Experiment: Exploring Fundamental Symmetries of the Universe. 2013.

[23] R. Acciarri et al. Long-Baseline Neutrino Facility (LBNF) and Deep Underground Neutrino Experiment (DUNE). 2016.

[24] R. Acciarri et al. Long-Baseline Neutrino Facility (LBNF) and Deep Underground Neutrino Experiment (DUNE). 2015.

[25] Soebur Razzaque and A. Yu. Smirnov. Super-PINGU for measurement of the leptonic CP-phase with atmospheric neutrinos. *JHEP*, 05:139, 2015.

[26] J. Alonso et al. Expression of Interest for a Novel Search for CP Violation in the Neutrino Sector: DAEdALUS. 2010.

[27] Emilio Ciuffoli, Jarah Evslin, and Fengyi Zhao. Neutrino Physics with Accelerator Driven Subcritical Reactors. *JHEP*, 01:004, 2016.

[28] Jun Cao et al. Muon-decay medium-baseline neutrino beam facility. *Phys. Rev. ST Accel. Beams*, 17:090101, 2014.

[29] Mattias Blennow, Pilar Coloma, and Enrique Fernndez-Martinez. The MOMENT to search for CP violation. *JHEP*, 03:197, 2016.

[30] Emilio Ciuffoli, Jarah Evslin, and Xinmin Zhang. The Leptonic CP Phase from Muon Decay at Rest with Two Detectors. *JHEP*, 12:051, 2014.

[31] David V. Forero and Patrick Huber. Hints for leptonic CP violation or New Physics? 2016.

[32] N. Klop and A. Palazzo. Imprints of CP violation induced by sterile neutrinos in T2K data. *Phys. Rev.*, D91(7):073017, 2015.

[33] Antonio Palazzo. 3-flavor and 4-flavor implications of the latest T2K and NOνA electron (anti-)neutrino appearance results. *Phys. Lett.*, B757:142–147, 2016.

[34] Raj Gandhi, Boris Kayser, Mehedi Masud, and Suprabh Prakash. The impact of sterile neutrinos on CP measurements at long baselines. *JHEP*, 11:039, 2015.

[35] Jiajun Liao, Danny Marfatia, and Kerry Whisnant. Degeneracies in long-baseline neutrino experiments from nonstandard interactions. *Phys. Rev.*, D93(9):093016, 2016.

[36] Mehedi Masud and Poonam Mehta. Non-standard interactions spoiling the CP violation sensitivity at DUNE and other long baseline experiments. 2016.

[37] Mehedi Masud, Animesh Chatterjee, and Poonam Mehta. Probing CP violation signal at DUNE in presence of non-standard neutrino interactions. 2015.

[38] Andr de Gouva and Kevin J. Kelly. Non-standard Neutrino Interactions at DUNE. *Nucl. Phys.*, B908:318–335, 2016.

[39] Pilar Coloma. Non-Standard Interactions in propagation at the Deep Underground Neutrino Experiment. *JHEP*, 03:016, 2016.

[40] Pouya Bakhti and Yasaman Farzan. CP-Violation and Non-Standard Interactions at the MO-MENT. 2016.

[41] Andr de Gouva and Kevin J. Kelly. False Signals of CP-Invariance Violation at DUNE. 2016.

[42] Mattias Blennow, Sandhya Choubey, Tommy Ohlsson, Dipyaman Pramanik, and Sushant K. Raut. A combined study of source, detector and matter non-standard neutrino interactions at DUNE. 2016.

[43] Pouya Bakhti and Amir N. Khan. Sensitivities to charged-current nonstandard neutrino interactions at DUNE. 2016.

[44] Jarah Evslin, Shao-Feng Ge, and Kaoru Hagiwara. The leptonic CP phase from T2(H)K and μ^+ decay at rest. *JHEP*, 02:137, 2016.

[45] Joachim Kopp, Manfred Lindner, Toshihiko Ota, and Joe Sato. Non-standard neutrino interactions in reactor and superbeam experiments. *Phys. Rev.*, D77:013007, 2008.

[46] Takashi Kikuchi, Hisakazu Minakata, and Shoichi Uchinami. Perturbation Theory of Neutrino Oscillation with Nonstandard Neutrino Interactions. *JHEP*, 03:114, 2009.

[47] A. De Rujula, M. B. Gavela, and P. Hernandez. Neutrino oscillation physics with a neutrino factory. *Nucl. Phys.*, B547:21–38, 1999.

[48] M. Freund, M. Lindner, S. T. Petcov, and A. Romanino. Testing matter effects in very long baseline neutrino oscillation experiments. *Nucl. Phys.*, B578:27–57, 2000.

[49] Evgeny K. Akhmedov. Matter effects in oscillations of neutrinos traveling short distances in matter. *Phys. Lett.*, B503:133–139, 2001.

[50] Paolo Lipari. CP violation effects and high-energy neutrinos. *Phys. Rev.*, D64:033002, 2001.

[51] Hisakazu Minakata and Hiroshi Nunokawa. Measuring leptonic CP violation by low-energy neutrino oscillation experiments. *Phys. Lett.*, B495:369–377, 2000.

[52] Hisakazu Minakata. The Three neutrino scenario. *Nucl. Phys. Proc. Suppl.*, 100:237–243, 2001.

[53] Osamu Yasuda. Vacuum mimicking phenomena in neutrino oscillations. *Phys. Lett.*, B516:111–115, 2001.

[54] O. L. G. Peres and A. Yu. Smirnov. Atmospheric neutrinos: LMA oscillations, U_{e3} induced interference and CP violation. *Nucl. Phys.*, B680:479–509, 2004.

[55] Mattias Blennow and Alexei Yu. Smirnov. Neutrino propagation in matter. *Adv. High Energy Phys.*, 2013:972485, 2013.

[56] Evgeny K. Akhmedov, A. Dighe, P. Lipari, and A. Y. Smirnov. Atmospheric neutrinos at Super-Kamiokande and parametric resonance in neutrino oscillations. *Nucl. Phys.*, B542:3–30, 1999.

[57] Hidekazu Yokomakura, Keiichi Kimura, and Akira Takamura. Overall feature of CP dependence for neutrino oscillation probability in arbitrary matter profile. *Phys. Lett.*, B544:286–294, 2002.

[58] Shao-Feng Ge, Kaoru Hagiwara, and Carsten Rott. A Novel Approach to Study Atmospheric Neutrino Oscillation. *JHEP*, 06:150, 2014.

[59] T. Wongjirad. Opportunities with Decay-at-rest Sources. *Neutrino 2016*.

[60] J. Beringer et al. Review of Particle Physics (RPP). *Phys. Rev.*, D86:010001, 2012.

[61] Katsuhiro Asano and Hisakazu Minakata. Large-Theta(13) Perturbation Theory of Neutrino Oscillation for Long-Baseline Experiments. *JHEP*, 06:022, 2011.

[62] Xun-Jie Xu. Why is the neutrino oscillation formula expanded in m_{21}^2 /m_{31}^2 still accurate near the solar resonance in matter? *JHEP*, 10:090, 2015.

[63] M. C. Gonzalez-Garcia and Michele Maltoni. Determination of matter potential from global analysis of neutrino oscillation data. *JHEP*, 09:152, 2013.

[64] Shao-Feng Ge, Pedro Pasquini, M. Tortola, and J. W. F. Valle. Measuring the Leptonic CP Phase in Neutrino Oscillations with Non-Unitary Mixing. 2016.

[65] Shao-Feng Ge. NuPro: a simulation package for neutrino properties. http://nupro.hepforge.org/.

[66] K. Abe et al. Neutrino oscillation physics potential of the T2K experiment. *PTEP*, 2015(4):043C01, 2015.